Dalton Transactions

PAPER

View Article Online
View Journal | View Issue

Cite this: *Dalton Trans.*, 2016, **45**, 5783

Electronic communication in phosphine substituted bridged dirhenium complexes – clarifying ambiguities raised by the redox non-innocence of the C_4H_2- and C_4-bridges†

Yan Li,[a] Olivier Blacque,[a] Thomas Fox,[a] Sandra Luber,[a] Walther Polit,[b] Rainer F. Winter,[b] Koushik Venkatesan[a] and Heinz Berke*[a]

The mononuclear rhenium carbyne complex *trans*-[Re(C≡CSiMe$_3$)(≡C–Me)(PMe$_3$)$_4$][PF$_6$] (**2**) was prepared in 90% yield by heating a mixture of the dinitrogen complex *trans*-[ReCl(N$_2$)(PMe$_3$)$_4$] (**1**), TlPF$_6$, and an excess of HC≡CSiMe$_3$. **2** could be deprotonated with KO*t*Bu to the vinylidene complex *trans*-[Re(C≡CSiMe$_3$)(=C=CH$_2$)(PMe$_3$)$_4$] (**3**) in 98% yield. Oxidation of **3** with 1.2 equiv. of [Cp$_2$Fe][PF$_6$] at –78 °C gave the C$_\beta$–C′$_\beta$ coupled dinuclear rhenium biscarbyne complex *trans*-[(Me$_3$SiC≡C)(PMe$_3$)$_4$Re≡C–CH$_2$–CH$_2$–C≡Re(PMe$_3$)$_4$(C≡CSiMe$_3$)][PF$_6$]$_2$ (**5**) in 92% yield. Deprotonation of **5** with an excess of KO*t*Bu in THF produced the diamagnetic *trans*-[(Me$_3$SiC≡C)(PMe$_3$)$_4$Re=C=CH–CH=C=Re(PMe$_3$)$_4$(C≡CSiMe$_3$)] complex (***E*-6(S)**) in 87% yield with an *E*-butadienediylidene bridge. Density functional theory (DFT) calculations of ***E*-6(S)** confirmed its singlet ground state. The *Z*-form of **6** (***Z*-6(S)**) could not be observed, which is in accord with its DFT calculated 17.8 kJ mol^{-1} higher energy. Oxidation of ***E*-6** with 2 equiv. of [Cp$_2$Fe][PF$_6$] resulted in the stable diamagnetic dicationic *trans*-[(Me$_3$SiC≡C)(PMe$_3$)$_4$Re≡C–CH=CH–C≡Re(PMe$_3$)$_4$(C≡CSiMe$_3$)][PF$_6$]$_2$ complex (***E*-6[PF$_6$]$_2$**) with an ethylenylidene dicarbyne structure of the bridge. The paramagnetic mixed-valence (MV) complex ***E*-6[PF$_6$]** was obtained by comproportionation of ***E*-6(S)** and ***E*-6[PF$_6$]$_2$** or by oxidation of ***E*-6(S)** with 1 equiv. of [Cp$_2$Fe][PF$_6$]. The dicationic *trans*-[(Me$_3$SiC≡C)(PMe$_3$)$_4$Re≡C–C≡C–C≡Re(PMe$_3$)$_4$(C≡CSiMe$_3$)][PF$_6$]$_2$ (**7[PF$_6$]$_2$**) complex, attributed a butynedi(triyl) bridge structure, was obtained by deprotonation of ***E*-6[PF$_6$]$_2$** with KO*t*Bu followed by oxidation with 2 equiv. of [Cp$_2$Fe][PF$_6$]. The neutral complex **7** could be accessed best by reduction of **7[PF$_6$]$_2$** with KH in the presence of 18-crown-6. According to DFT calculations **7** possesses two equilibrating electronic states: diamagnetic **7(S)** and triplet **7(F)** with ferromagnetically coupled spins. The latter is calculated to be 5.2 kcal mol^{-1} lower in energy than **7(S)**. There is experimental evidence that **7(S)** prevails in solution. **7** could not be isolated in the crystalline state and is unstable transforming mainly by H-abstraction to give ***E*-6(S)**. UV-Vis-NIR spectroscopy for the dinuclear rhenium complexes ***E*-6(S)**, ***E*-6[PF$_6$]** and ***E*-6[PF$_6$]$_2$**, as well as EPR spectroscopic and variable-temperature magnetization measurements for the MV complex ***E*-6[PF$_6$]** were also conducted. Spectro-electrochemical reduction studies on **7[PF$_6$]$_2$** allowed the characterization of the mono- and direduced forms of **[7]$^+$** and **7** by means of IR- and UV-Vis-NIR-spectroscopy and revealed the chemical fate of the higher reduced form.

Received 7th December 2015,
Accepted 18th February 2016

DOI: 10.1039/c5dt04768d

www.rsc.org/dalton

I. Introduction

Organometallic rigid-rod dinuclear complexes consisting of a rigid π-conjugated organic carbyl or hydrocarbyl bridge C$_x$H$_y$ with redox-active metal end groups of the type [L$_n$MC$_x$H$_y$ML$_n$] (M = metal; L = ligand) have recently received considerable attention due to their potential function in molecular electronic devices.[1] In this paper we will address the tetracarbyl (C$_4$) and butadiene-1,4-di(ylidene) (C$_4$H$_2$) units as rigid π-conjugated bridging moieties of rhenium based complexes. Rigid molecules of these kinds are denoted as molecular wires

[a]*Department of Chemistry, University of Zurich, Winterthurerstrasse 190, CH-8057 Zurich, Switzerland. E-mail: hberke@chem.uzh.ch*
[b]*Fachbereich Chemie der Universität Konstanz, Universitätstrasse 10, D-78457 Konstanz, Germany*

†Electronic supplementary information (ESI) available: Experimental details describing the syntheses as well as giving details of the NMR spectroscopy, refinement details and crystallographic data for the X-ray diffraction studies, deconvoluted UV-Vis-NIR spectra and computational results. CCDC 859304–859309. For ESI and crystallographic data in CIF or other electronic format see DOI: 10.1039/c5dt04768d

potentially providing molecular conductance between the remote ends.[1,2] For instance, Gladysz and co-workers reported a series of dinuclear rhenium complexes with μ-C_x carbyl chains ($x \leq 20$) composed of up to ten alkynyl units.[3] Voltammetric studies revealed that with increasing chain lengths, the potential difference $\Delta E_{1/2}$ between the two mainly metal derived redox processes decreases and the oxidation becomes increasingly irreversible. In other words, the longer the chain length, the smaller is the electronic interaction between the remote redox sites and the higher is the reactivity of the (hydro)carbyl chain. The HOMO and LUMO of bridged polyacetylenic systems ([$L_nMC_xML_n$], x = even number) are in most cases π-type molecular orbitals with only limited π-delocalization, large HOMO–LUMO gaps, and quite low polarizabilities of the bridges also preventing strong metal–bridge–metal interactions. Furthermore, for molecules serving as junctions in single-molecule conductivity devices the energetic alignment of the HOMO or the LUMO with the Fermi level E_F of the metal electrodes favors electron transfer *via* a resonant conductance mechanism.[4] This conductance mechanism can be addressed by cyclic voltammetry (CV) and by UV-Vis-NIR spectroscopy. Here the interaction of the metal centers can be quantified on the basis of the characteristic parameters (energy $\tilde{\nu}$, extinction coefficient ε and band-width at half height $\Delta\tilde{\nu}_{1/2}$) of the intervalence charge transfer (IVCT) absorptions of dinuclear mixed-valence complexes.[23,24] According to their interaction strengths mixed-valence systems have been grouped into three classes by Robin & Day[5] and an extension of this view has been given with regard to charged species by Kaupp *et al.*[6]

The through-bridge electronic interaction in dinuclear complexes has a significant impact on their chemical and physical properties, which greatly depends on the type of metal centers, the ancillary ligands and the bridge.[2t,3,7] Based on the ease of synthetic access, stability, and favorable electronic properties, the relatively short butadiene-1,4-di(ylidene) C_4H_2 and butadiynediyl C_4 chains were anticipated to be appropriate bridges for strong electronic interactions between the metal centers.[3] Therefore intensive investigations have been carried out on complexes of the type [$L_nMC_4ML_n$] with different transition metal centers, such as Mn,[8] Fe,[3a,9] Re,[10] Ru,[11] Pt,[12] W, and Mo.[13] However, only complexes with metal centers, which could take over the role of bi- or trifunctionalized linking units possess the potential for the build-up of oligo- or polynuclear complexes. Mono-functionalized bridged metal centers are functioning as end groups and are in connectivity terms stopper units. In addition bi- or trifunctionalized metal centers would allow the introduction of special types of functionalities for, for instance, their hook up to electrodes, which is the key to their function as junctions in molecular conductance devices.

Therefore we sought to construct *trans*-bifunctional dinuclear rhenium complexes equipped with C_4H_2 and C_4 bridges and a trimethylsilyl acetylide functional group, the latter eventually enabling a stable and electronically strong coupling to gold electrodes as previously demonstrated in the case of organic oligoynes[14,15] and of appropriate dinuclear complexes by pre-measurement removal of the silyl groups[16] or by subsequent conversion of the silyl into stannyl groups, which allow spontaneous removal of the tin groups upon contact with the gold surface.[2b,c,16b]

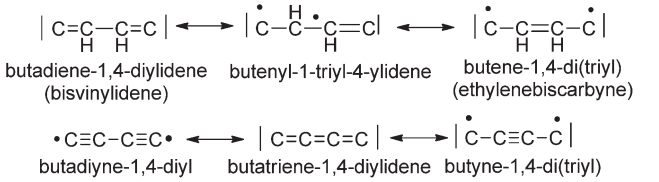

Scheme 1 Different canonical forms of the C_4H_2 and the C_4 ligand bridges.

The C_4H_2 and C_4 bridges belong to the class of redox non-innocent ligands[17] and are by this property expected to enable the terminal binding of metal centers by various canonical forms (Scheme 1). These bridges are prone to electronic flexibility in their σ- and π-bonding adjusting electronically *via* varying electron counts at the bridges' termini. It would be natural to assume that in the case of metal attachment the C_2H_4 or C_4 bridging systems adopt to the electron demands of electron-precise metal centers. The bridges' π electrons are variably distributed between CC π bonding electrons and electrons π donated to the metal centers. The π electrons donated to a metal center account for varying strengths of the metal–carbon bonds and the π electrons of the bridge account for different π stabilizations within the bridges (Scheme 1).

For instance, the butadiyne-1,4-diyl bridging unit is expected to have the lowest π-delocalization between the metal centers[13a,18] of all possible forms of the C_4 bridge, since the number of π electrons donated to the metal centers is zero and the π-delocalization of diynes is quite low.[19,20]

In special cases, when the M–C bond is strongly covalent, the bridging ligands will sometimes not adjust to the electron demand of the metal centers. This in turn might lead to ligand-dominated redox-processes and the so-called "non-innocent" behaviour.[17,21] It maybe interesting to note that the isomeric forms of the C_4H_2 and the C_4 bridge are expected to be related by bond-stretch isomerism revealing different carbon–carbon bond lengths as free molecules and as ligands in complexes.[22]

For the development of dinuclear complexes with conjugated C_4H_2 and C_4 bridges we selected the 16e$^-$ rhenium fragment [(RC≡C)$(PMe_3)_4$Re], which is bifunctional in the sense that it allows for hooking up to electrodes *via* the RC≡C group and can act at the same time as one terminus of bridging systems. The targeted dinuclear rhenium complexes were anticipated to be analogous to manganese-based ones reported by our group earlier and to be related to systems with [X(diphosphine)$_2$W] end groups possessing one electron less per metal site. Both types of systems should therefore differ in the preferred canonical form of the bridge and in their electronic properties.[8,13c,23] Rhenium as a heavier transition element was expected to render structurally stable complexes and to form

strong ligand bonds concomitant with higher barriers for ligand exchange. To avoid difficulties in the synthetic access to $[L_nReC_4H_2ReL_n]$ and $[L_nReC_4ReL_n]$ complexes, we tried to circumvent the direct introduction of the C_4H_2 and C_4 bridges by ligand exchange by the alternative construction of μ-C_4H_n (n = 0, 2 or 4) dinuclear complexes by oxidative C–C coupling processes, *i.e.* by 'dimerizing' mononuclear C_2H_n (n = 0, 1 or 2) complex units. Our work on manganese coupling chemistry[8a,23a,b,e,f,24] and related work on niobium,[25] tungsten,[13a] molybdenum,[13a,26] manganese,[18a,27] rhenium,[28] iron,[9,29,34] and ruthenium[30] complexes demonstrated the synthetic utility of the oxidative coupling of metal alkynyls or of oxidative dehydro-dimerizations of metal vinylidenes.[18b,31]

A key point of our rhenium based endeavors to access dinuclear rhenium complexes of the type $[(Me_3SiC{\equiv}C)(PMe_3)_4ReC_4H_nRe(PMe_3)_4(C{\equiv}CSiMe_3)]$ with n = 0, 2 or 4 was thus to synthetically access the mononuclear rhenium vinylidene species *trans*-$[Re(C{\equiv}CSiMe_3)(=C=CH_2)(PMe_3)_4]$ and couple that complex to the non-conjugated C_4H_4 bridged system. From there we sought to access the C_4H_2 and C_4 bridges by successive oxidative dehydrogenations.

II. Results and discussion

IIa. Synthesis and characterization of mononuclear rhenium complexes

The synthesis of the dinuclear rhenium complex *trans*-$[(Me_3SiC{\equiv}C)(PMe_3)_4Re{\equiv}C{-}CH_2{-}CH_2{-}C{\equiv}Re(PMe_3)_4(C{\equiv}CSiMe_3)][PF_6]_2$ started from the dinitrogen complex *trans*-$[ReCl(N_2)(PMe_3)_4]$ (**1**). From this precursor the mononuclear rhenium carbyne complex *trans*-$[Re(C{\equiv}CSiMe_3)({\equiv}CMe)(PMe_3)_4][PF_6]$ (**2**) was formed in 90% yield by heating in a 1 : 1 mixture with $TlPF_6$ and by the addition of excess $HC{\equiv}CSiMe_3$ in *N*,*N*-diisopropylethylamine (DIPEA)/THF at 95 °C (Scheme 2).

The mononuclear rhenium carbyne complex **2** readily underwent deprotonation using excess KO*t*Bu in THF to form the corresponding mononuclear rhenium vinylidene complex *trans*-$[Re(C{\equiv}CSiMe_3)(=C=CH_2)(PMe_3)_4]$ (**3**) in 98% yield[18b,31c] (Scheme 2). Re-protonation of **3** could be accomplished using HCl to recover the carbyne complex *trans*-$[Re(C{\equiv}CSiMe_3)({\equiv}C{-}Me)(PMe_3)_4]Cl$ (**4**) as a chloride salt, which in turn could be deprotonated with KO*t*Bu to regenerate **3**.

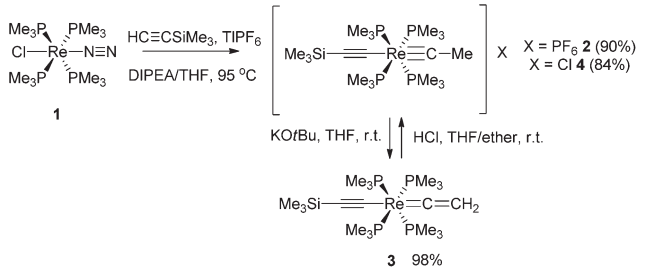

Scheme 2

The mononuclear rhenium complexes **2**, **3** and **4** were characterized by NMR, IR, elemental analyses and mass spectroscopy. The ^1H NMR spectrum of *trans*-$[Re(C{\equiv}CSiMe_3)(=C=CH_2)(PMe_3)_4]$ (**3**) displayed a characteristic quintet for the vinylidene protons at 1.35 ppm ($^4J_{PH}$ = 3.5 Hz). In the $^{13}C\{^1H\}$ NMR spectrum two resonances were found at 301.6 ppm ($^2J_{PC}$ = 11.9 Hz) and 87.8 ppm that could be assigned to the C_α and C_β atoms of the vinylidene group. The other two resonances at 150.1 ppm and 67.8 ppm were attributed to the C_α and C_β atoms of the acetylide moiety[8a,18,23a,b,f,27,28] presumably reflecting an extraordinary electron-richness. The IR spectrum of **3** showed strong ν(C=C) and ν(C≡C) bands at 1558 and 1982 cm^{-1}, respectively.

The carbyne complexes *trans*-$[Re(C{\equiv}CSiMe_3)({\equiv}C{-}Me)(PMe_3)_4][PF_6]$ (**2**) and *trans*-$[Re(C{\equiv}CSiMe_3)({\equiv}C{-}Me)(PMe_3)_4]Cl$ (**4**) exhibited in the ^1H NMR spectra a characteristic quintet for the $Me_{carbyne}$ protons at 1.27 ppm ($^4J_{PH}$ = 4.0 Hz) and 1.31 ppm ($^4J_{PH}$ = 4.0 Hz), respectively, while the $^{13}C\{^1H\}$ NMR spectra of **2** and **4** displayed respective resonances for the C_α atoms at 284.5 or 284.9 ppm. Their intensity was, however, too low to allow extraction of the apparently small J_{PC} values. Two additional $^{13}C\{^1H\}$ NMR resonances at 134.7 and 125.7 ppm or at 135.0 ppm and 125.8 ppm for **2** and **4** confirmed the presence of the acetylide groups. In the IR spectra ν(C≡C) bands for **2** and **4** were observed at 2029 cm^{-1} or 2025 cm^{-1}, respectively. A singlet resonance in the $^{31}P\{^1H\}$ NMR spectra complied with the *trans*-arrangements of the alkynyl and carbyne ligands in **2**, **3** and **4**.

IIb. Synthesis and characterization of C_4H_n bridged dirhenium complexes

Oxidative C–C coupling was demonstrated to be an effective method for the build-up of the bridges of dinuclear μ-C_4H_2 and μ-C_4 complexes.[18a,23a,b,f,27,28,30] To adjust this method to dinuclear rhenium complexes with C_4H_2 bridges, we initially tried a variation of the oxidative coupling of **3** with electron and proton removal in the presence of a base. However, the reaction of **3** with $[Cp_2Fe][PF_6]$ in the presence of quinuclidine, DBU, or KO*t*Bu inevitably resulted in a mixture of complexes: the mononuclear rhenium carbyne complex *trans*-$[Re(C{\equiv}CSiMe_3)({\equiv}C{-}Me)(PMe_3)_4][PF_6]$ (**2**), the dinuclear rhenium biscarbyne complex *trans*-$[(Me_3SiC{\equiv}C)(PMe_3)_4Re{\equiv}C{-}CH_2{-}CH_2{-}C{\equiv}Re(PMe_3)_4(C{\equiv}CSiMe_3)][PF_6]_2$ (**5**), and the dicationic bisvinylidene complex *trans*-$[(Me_3SiC{\equiv}C)(PMe_3)_4Re{=}C{=}CH{-}CH{=}C{=}Re(PMe_3)_4(C{\equiv}CSiMe_3)][PF_6]_2$ (**6[PF$_6$]$_2$**). This complex reaction behavior was partly attributed to the highly basic nature of **3**, which competed with the base added to deprotonate the oxidatively formed radical cation $[\mathbf{3}]^+$ giving **2** and the acetylide complex *trans*-$[(Me_3SiC{\equiv}C)Re(C{\equiv}C{-}Me)(PMe_3)_4]$ and, by subsequent oxidation, the *trans*-$[(Me_3SiC{\equiv}C)Re(C{\equiv}CMe)(PMe_3)_4]^+$ cation, which dimerized by C–C coupling to give **6[PF$_6$]$_2$**. We anticipated that a better control of the resulting products could be achieved by performing the reaction in the absence of a base at low temperatures[27] to accumulate $[\mathbf{3}]^+$ at higher concentrations, thus promoting the second order recombination reaction to **5**. Oxidation of **3** was carried out at

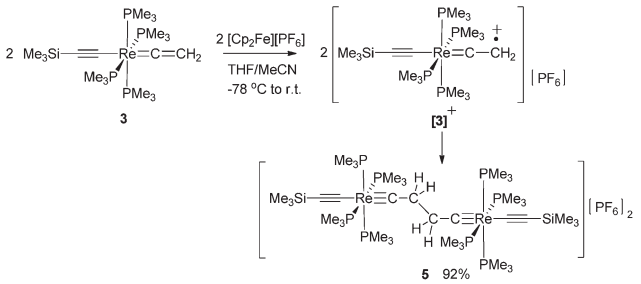

Scheme 3

−78 °C by adding a THF solution of **3** dropwise to an excess of $[Cp_2Fe][PF_6]$ in CH_3CN/THF (1 : 3 ratio) leading to a 92% yield of the coupled dicationic dirhenium biscarbyne complex *trans*-$[(Me_3SiC{\equiv}C)(PMe_3)_4Re{\equiv}C{-}CH_2{-}CH_2{-}C{\equiv}Re(PMe_3)_4(C{\equiv}CSiMe_3)][PF_6]_2$ (**5**) as the sole product (Scheme 3).

The ^1H NMR spectrum of **5** displayed three signals. A resonance at 1.56 ppm was ascribed to the CH_2 protons of the bridge and two other signals at 1.75 ppm and 0.05 ppm were attributed to the protons of the PMe_3 and the $SiMe_3$ groups, respectively. In the $^{13}C\{^1H\}$ NMR spectrum resonances appeared for the C_α and C_β atoms of the μ-biscarbyne ligand at 279.9 ppm ($^2J_{PC}$ = 13.8 Hz) and 46.4 ppm. Two additional resonances of the $^{13}C\{^1H\}$ NMR spectrum at 134.0 ppm ($^2J_{PC}$ = 19.4 Hz) and 126.6 ppm were attributed to the terminal acetylide groups; additionally a $\nu(C{\equiv}C)$ band at 2027 cm^{-1} in the IR spectrum was also diagnostic for that moiety. In the ^{31}P NMR spectrum the resonance for the PMe_3 ligands appeared at −42.2 ppm, while the $[PF_6]^-$ anion gave rise to a septet at −146.6 ppm. The composition of **5** was confirmed by a correct elemental analysis.

5 could be deprotonated by applying an excess of KO*t*Bu yielding the brownish-green bisvinylidene complex *E*-$[(Me_3SiC{\equiv}C)(PMe_3)_4Re{=}C{=}CH{-}CH{=}C{=}Re(PMe_3)_4(C{\equiv}C\text{-}SiMe_3)]$ (***E*-6(S)**) in 87% yield (Scheme 4). The use of lithium diisopropylamide (LDA) as a base at room temperature in THF furnished a somewhat lower yield (83%), but the work-up procedure to ***E*-6(S)** was found to be more facile in this case. It is

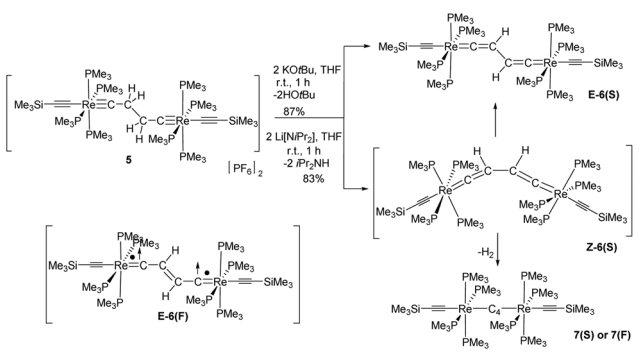

Scheme 4 Synthesis of ***E*-6(S)** *via* deprotonation of **5**. Generation, isomerization and dehydrogenation of the potential intermediate complex ***Z*-6(S)**. Sketch of ***E*-6(F)** as an activated state of ***E*-6**.

quite remarkable that the *Z*-isomer ***Z*-6(S)** could not be traced at any stage of the reaction to **5**. ***Z*-6(S)** might indeed form in these reactions. Kohn–Sham density functional theory (DFT) calculations indicate that ***Z*-6(S)** is at a high energy of 17.8 kcal mol^{-1} above ***E*-6(S)** and transforms quickly into ***E*-6(S)** (see section III). An alternative deactivation pathway of ***Z*-6(S)** could be its dehydrogenation (***Z*-6(S)** → **7(F)** + H_2) assuming a low activation barrier for this process (Scheme 6). The latter process was calculated by DFT to be energetically downhill by −7.8 kcal mol^{-1}. In this context it should be mentioned that the dehydrogenation reaction of ***E*-6(S)** (***E*-6(S)** → **7(F)** + H_2) was calculated to be energetically uphill by 10.0 kcal mol^{-1} and is therefore anticipated not to occur. The ***Z*-6(S)** dehydrogenation process to **7(F)** could make up for the 13 or 17% of the missing yield of ***E*-6(S)** in its formation process along Scheme 4. It should be mentioned at this point that the open-shell structure ***E*-6(F)** with ferromagnetically coupled electrons is an excited state of ***E*-6(S)** at a too high electronic energy to be reached by thermal activation and is therefore expected to be non-existent at room temperature in solution.

The ^1H NMR spectrum of ***E*-6(S)** in THF-d_8 at room temperature revealed a 'normal' $H_{vinylidene}$ chemical shift of 2.50 ppm; but its doublet structure (J = 4 Hz) was unexpected and indicated a peculiar phenomenon. The solid state structure of ***E*-6(S)** (Fig. 1a) possesses an approximate planarity of the [Re]═C═CH–CH═C═[Re] moiety. On this basis, the mentioned coupling can be interpreted as $^4J_{PH}$ coupling originating from the *trans*-coplanar arrangement of the closest $H_{vinylidene}$ atom (plane ($H_{vinylidene}$, C2, C1)) to the strongly 'bent-back' P3 atom (plane (P3, Re, C1) of Fig. 1a and Scheme 5). The coupling effect would be strongest, if the ReP_4 fragment is subject

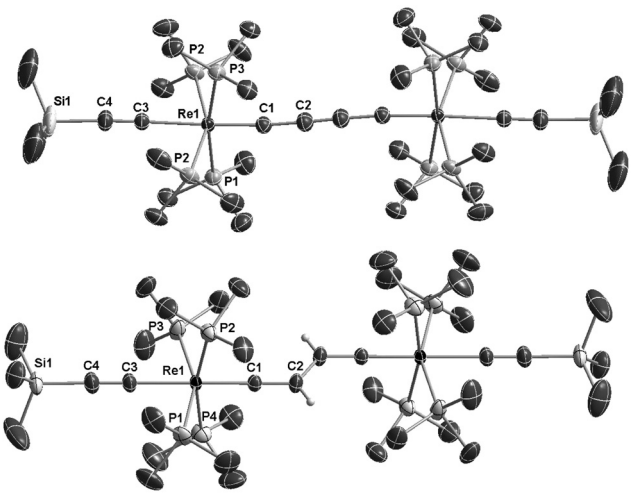

Fig. 1 ORTEP like drawing of (a) of the neutral dinuclear rhenium butadienediylidene complex *trans*-$[(Me_3SiC{\equiv}C)(PMe_3)_4ReC_4H_2Re(PMe_3)_4(C{\equiv}CSiMe_3)]$ (***E*-6(S)**) (bottom); (b) of the dicationic dinuclear rhenium complex *trans*-$[(Me_3SiC{\equiv}C)(PMe_3)_4Re{\equiv}C{-}C{\equiv}C{-}C{\equiv}Re(PMe_3)_4(C{\equiv}CSiMe_3)][PF_6]_2$ **7[PF$_6$]$_2$** (top) (50% probability level of thermal ellipsoids; solvate molecules, the $[PF_6]^-$ counterions and selected hydrogen atoms are omitted for clarity).

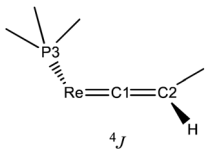

Scheme 5 Sketch of the *trans*-coplanar arrangement of P3 with $H_{vinylidene}$ of ***E*-6(S)**.

to hindered rotation, which prevents averaging on the NMR time scale with the other three non-coupled P atoms ($^4J_{PH} = 0$).

The ^{13}C, ^{31}P and ^{29}Si NMR signals of ***E*-6(S)** are in agreement with the presence of a diamagnetic compound. In the $^{13}C\{^1H\}$ NMR spectrum of ***E*-6(S)** in THF-d_8 at 10 °C two characteristic signals appeared, which were assigned to the C_α and C_β vinylidene atoms at 309.4 ppm (quint, $^2J_{PC} = 12.8$ Hz) and 96.7 ppm. Two additional resonances at 152.8 ppm ($^2J_{PC} = 16.0$ Hz) and 127.8 ppm were attributed to the C_α and C_β atoms of the acetylide groups. The ^{31}P and the ^{29}Si NMR spectra showed singlet resonances of ***E*-6(S)** at $\delta = -40.5$ ppm (^{31}P NMR) and at $\delta = -31.8$ ppm (^{29}Si NMR).

The solid state IR and Raman spectra displayed a strong ν(C≡C) band at 1975 cm^{-1} (IR) or 1973 cm^{-1} (Raman) for the terminal acetylide moieties. Bands at 1543 cm^{-1} (IR) and 1581 cm^{-1} (Raman) were attributed to the ν_{as}(CCHCHC) vibration of the bridge (IR) and to the corresponding ν_s(CCHCHC) vibration (Raman). The molecular structure of ***E*-6(S)** obtained by single crystal X-ray diffraction (*vide infra*) also demonstrated the *E*-configuration for this molecule and, moreover, the bond distances in the bridge reflected the singlet state of the butadiene-1,4-diylidene(bisvinylidene) canonical form (Scheme 1).

As shown in Scheme 6 ***E*-6(S)** could be oxidized by two equiv. of $[Cp_2Fe][PF_6]$ to yield the diamagnetic dicationic complex *E*-$[(Me_3SiC{\equiv}C)(PMe_3)_4Re{\equiv}C{-}CH{=}CH{-}C{\equiv}Re(PMe_3)_4(C{\equiv}CSiMe_3)][PF_6]_2$ (***E*-6[PF$_6$]$_2$**) preserving the *E*-configuration, but adopting an ethylenylidene dicarbyne canonical structure of the bridge (see also X-ray diffraction study of ***E*-6[PF$_6$]$_2$** summarized in Table 1 and displayed in the ESI†) The ^1H NMR spectrum of ***E*-6[PF$_6$]$_2$** showed a unique resonance for both vinylidene protons at 5.82 ppm in the typical chemical shift range of olefinic protons, but in a shift range distinct from the corresponding resonances of ***E*-6(S)** indicating a significantly different electronic structure. ***E*-6[PF$_6$]$_2$** revealed resonances for the C_α and C_β nuclei at 265.3 ppm and 145.8 ppm, again appearing in a chemical shift range distinct from that of ***E*-6(S)**. Due to their low intensities we could not extract the J_{PC} values. Additional ^{13}C NMR resonances at 135.5 ppm and 130.9 ppm were attributed to the acetylide groups. In the ^{31}P NMR spectrum a resonance at −43.8 ppm was ascribed to the P nuclei of the PMe_3 ligands. The characteristic signal for the $[PF_6]^-$ anion appeared as a septet at −143.9 ppm. Although reduction of ***E*-6[PF$_6$]$_2$** to ***E*-6(S)** could be carried out with an excess of Na/benzophenone, this reaction was achieved with better control using lithium diisopropylamide (LDA) acting initially as a hydride transfer agent leading to dimethylisopropyl imine[32] and the hydride added putative intermediate species **5[PF$_6$]**, which becomes subsequently deprotonated by LDA to form ***E*-6(S)** (Scheme 6).

The comproportionation reaction of ***E*-6(S)** with ***E*-6[PF$_6$]$_2$** or the oxidation of ***E*-6(S)** with one equiv. of $[Cp_2Fe][PF_6]$ produced the stable mixed valence complex ***E*-6[PF$_6$]** (Scheme 5). Only broad signals were observed in the ^1H NMR spectra for ***E*-6[PF$_6$]** indicating paramagnetic behavior. For ***E*-6[PF$_6$]** and the dicationic species ***E*-6[PF$_6$]$_2$**, the IR spectra showed weak acetylenic bands at 1987 cm^{-1} and 2022 cm^{-1}, respectively. In the Raman spectra the corresponding bands were assigned at 2001 cm^{-1} and 2017 cm^{-1}. $\nu(C_4)$ bands of the C_4H_2 bridge could not be observed for ***E*-6[PF$_6$]** and ***E*-6[PF$_6$]$_2$** in the IR. In the case of ***E*-6[PF$_6$]** this can be viewed as an indication of strong electron delocalization on the IR time scale (10^{-13} s).[13c] The diamagnetic dicationic ethylenylidene biscarbyne complex ***E*-6[PF$_6$]$_2$** showed good solubility and stability in polar solvents, such as CH_2Cl_2 and MeCN. In contrast, neutral ***E*-6(S)** complexes and monocationic ***E*-6[PF$_6$]** decomposed quickly in CH_2Cl_2, and over longer period of times also in MeCN, and they underwent facile oxidation in the solid state and in solution. ***E*-6(S)** is stable for several months under an inert atmosphere, but should be stored as a solid at −30 °C.

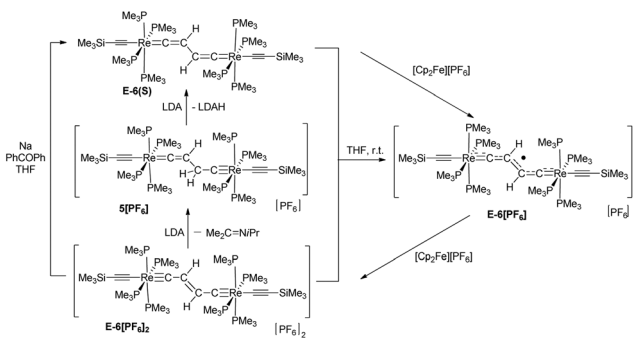

Scheme 6 Redox reactions of ***E*-6(S)**, ***E*-6[PF$_6$]** and ***E*-6[PF$_6$]$_2$** and comproportionation of ***E*-6(S)** and ***E*-6[PF$_6$]$_2$** to yield ***E*-6[PF$_6$]**.

IIc. Characterization of C_4 bridged dirhenium complexes

The dicationic *trans*-$[(Me_3SiC{\equiv}C)(PMe_3)_4ReC_4Re(PMe_3)_4(C{\equiv}C\text{-}SiMe_3)][PF_6]_2$ complex (**7[PF$_6$]$_2$**) could be obtained by repetitive cycles of deprotonations and oxidations starting from ***E*-6[PF$_6$]$_2$** or from **2** following method a or method b as depicted in Scheme 7.

In the ^1H NMR spectrum the dicationic complex **7[PF$_6$]$_2$** showed singlet resonances for the PMe_3 ligands at 1.82 ppm and for the trimethylsilyl groups at 0.26 ppm. The $^{13}C\{^1H\}$ NMR spectrum revealed characteristic resonances for C_α and C_β at 235.0 and 95.8 ppm, but the intensities of these signals were too low to extract J_{PC} couplings. The resonances of the acetylide groups appeared at 135.5 ppm and 128.4 ppm. In the ^{31}P NMR spectrum a singlet resonance at −43.6 ppm was ascribed to the PMe_3 ligands. The characteristic signal for the $[PF_6]^-$ counterion appeared as a septet at −143.9 ppm. The

Table 1 Selected bond lengths [Å] and angles [°] for **5**, ***E*-6(S)**, ***E*-6[PF$_6$]**, ***E*-6[PF$_6$]$_2$** and **7[PF$_6$]$_2$**. Assignment of the bond lengths in the C_4 bridge follows the notation: C4C3[Re]C1C2C2′C1′[Re′]C3′C4′ '*trans*' phosphines; ** BHLYP (in brackets: B3LYP); see section III and the ESI

Bond	**5**	***E*-6(S)**	***E*-6(S)** DFT**	***E*-6[PF$_6$]**	***E*-6[PF$_6$]$_2$**	**7(S)** DFT**	**7(F)** DFT**	**7[PF$_6$]$_2$**
Re1–C1	1.7834 (19)	1.904 (2)	1.899 (1.912)	1.851 (6)	1.805 (5)	1.943 (1.965)	2.038 (1.972)	1.814 (4)
C1–C2	1.491 (3)	1.337 (3)	1.322 (1.333)	1.375 (8)	1.414 (7)	1.270 (1.276)	1.234 (1.274)	1.363 (5)
C2–C2′	1.513 (4)	1.469 (4)	1.462 (1.465)	1.388 (10)	1.331 (10)	1.295 (1.305)	1.345 (1.301)	1.197 (8)
P1–Re1–P3*	156.20 (2)	155.45 (2)	155.24 (155.14)	156.49 (6)	170.3 (4)	164.27 (163.86)	164.16 (163.32)	169.20 (3)
P5–Re2–P7*	—	—		156.46 (6)	—			—
P2–Re–P4*	171.22 (2)	165.36 (2)	163.89 (163.61)	166.62 (6)	155.7 (4)	155.20 (155.33)	157.76 (160.20)	155.13 (4)
P6–Re–P8*	—	—		166.71 (6)	—			—
Re···Re	7.323	7.416	7.348 (7.400)	7.371	7.282	7.718 (7.786)	7.915 (7.797)	7.536

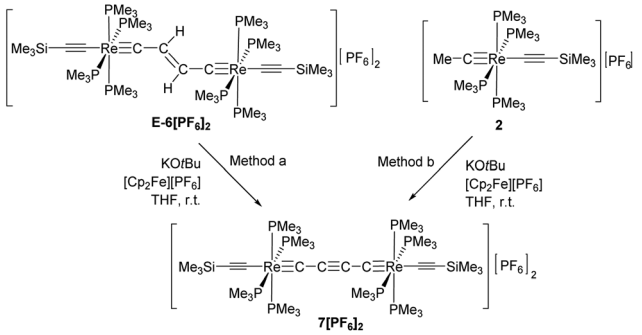

Scheme 7

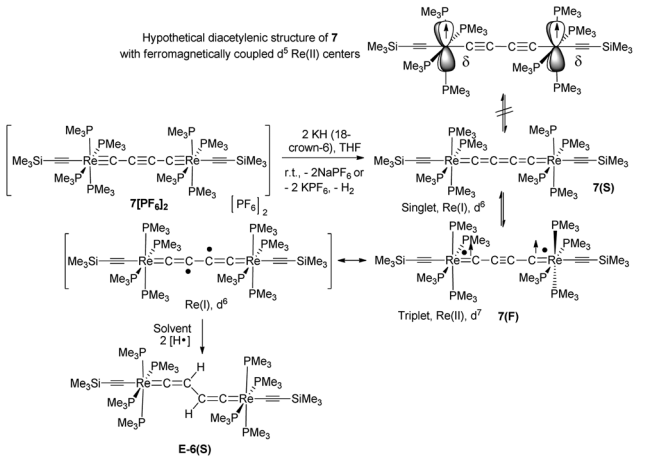

Scheme 8 Synthesis, possible electronic structures, and hydrogen abstraction of the isomers of **7** (**7(F)** and **7(S)**).

IR spectrum of **7[PF$_6$]$_2$** revealed a weak band at 2013 cm^{-1} attributed to a vibrational band of the acetylenic substituents. Vibrational bands for the C_4 moiety could not be found, which supports the notion of a highly symmetric bridging unit of **7[PF$_6$]$_2$**.

The reduction of the dicationic species **7[PF$_6$]$_2$** was attempted by treatment with Na/Hg or Na/benzophenone, but these reactions resulted in a mixture of many components. Using KH in the presence of 18-crown-6 in THF the neutral *trans*-[(Me$_3$SiC≡C)(PMe$_3$)$_4$ReC$_4$Re(PMe$_3$)$_4$(C≡CSiMe$_3$)] complex **7** was formed. As depicted in Scheme 7 and according to DFT calculations (section III), two different electronic structures have to be considered for **7**: diradical **7(F)** with a but-2-ynediylidene bridge and with ferromagnetically coupled electrons and diamagnetic **7(S)** with a butatrienediylidene bridge. The unpaired spins of **7(F)** would be delocalized over the entire ReC$_4$Re moiety and occupy two degenerate perpendicular π orbitals, which according to Hund's rule should lead to a ferromagnetic electronic state. **7(S)** possesses a cumulenic bridge (Scheme 1) providing 2-electrons to each electron-precise Re(I) center, thus establishing a diamagnetic molecule. The MO description of the cumulenic structure is particularly complex, since it is based on different occupancies of the two π planes of the bridge. The inequality of these π planes becomes further amplified in the complex **7(S)** by interaction with the unequal π planes of the rhenium centers strongly distinguished in their binding capacity *via* dislocation of the PMe$_3$ ligands from planarity (section IId). These electronic states of **7** are expected to co-exist at room temperature in solution. However, experimentally it was not possible to distinguish these isomers or to determine the ratio at which these isomers equilibrate.

It should be mentioned at this point that another conceivable isomeric form of **7** is based on a diacetylenic canonical form of the bridge (Schemes 1 and 8). The diacetylenic bridge would need to formally accept one σ electron from each rhenium center to form a diacetylide ligand bridging two low-spin d^5 Re(II) fragments with δ type singly occupied d-orbitals.[33] The δ type d-orbitals would be arranged perpendicular to the main axis of the molecule incapable of interacting with π-type orbitals of the bridge and excluding conjugation. These remote radical centers could therefore coexist in this isomer of **7** as ferromagnetically coupled SOMOs (Scheme 8). However, according to the DFT calculations in section III the δ orbitals of such rhenium based complexes are located within the "t_{2g}" set at relatively low energies well below the HOMO/SOMO levels. An isomer of **7** with a diacetylenic bridge is therefore very unlikely and is thus omitted from the subsequent discussion.

7 is indeed quite unstable and very reactive reflecting either the high nucleophilicity and basicity of **7(S)** or the open-shell diradical character of **7(F)**. Various attempts to isolate **7** failed. At room temperature in solution the main decomposition product was found to be **6(S)**, which is likely formed through

H-abstraction from the solvent by any form of **7** (Scheme 7). Formally this reaction could be envisaged to occur preferably with **7(F)** in a resonance structure with radical centers at C_β and C'_β. H-abstraction of **7** to form ***E*-6(S)** could further be substantiated by spectro-electrochemical studies (*vide infra*) identifying ***E*-6(S)** as a subsequent product of **7** by IR and UV-Vis spectroscopy (section IVc). Nuclei in close vicinity to radical centers are excluded from NMR identification due to paramagnetic broadening and shifting of the signals. Therefore, in **7(F)** only NMR signals of atoms distant to the radical centers may be observable as broadened or somewhat broadened resonances. In solutions of **7** slightly broadened ^{1}H NMR resonances could be detected at 1.10 and 0.53 ppm, which were assigned to the protons of the Me_P and Me_{Si} groups, respectively, but the ^{29}Si spectrum showed only a very broad signal and ^{13}C NMR and ^{31}P NMR signals could not be observed at all. The ^{1}H NMR signal broadening of the methyl resonances of **7** was, however, rather low. From these observations we conclude that, in solution, **7(S)** is the prevalent species, coexisting with **7(F)**, rapidly equilibrating at room temperature on the NMR time scale. Additional evidence for the prevalence of **7(S)** as the main solution component of **7** was derived from the spectro-electrochemical studies (*vide infra*) in THF. For instance, the appearance and position of a cumulenic type $\nu(C_4)$ IR band at 1758 cm^{-1} speaks for the existence of **7(S)** in solutions of **7**. We note here that for the related complex [(η^5-MeC_5H_4)(dmpe)MnC≡CMn(dmpe)(η^5-MeC_5H_4)] diamagnetic and paramagnetic states have also been postulated to equilibrate in solution.[23c]

It should be mentioned at this point that in particular the spectro-electrochemical studies (section IVc) provided clear evidence that the mono-oxidized species **7[PF$_6$]** is existent in solution.

IId. Structural features of the [P_4Re]C_4H_2[ReP_4] and [P_4Re]C_4[ReP_4] units of 5, *E*-6(S), *E*-6[PF$_6$], *E*-6[PF$_6$]$_2$ and 7[PF$_6$]$_2$

The dinuclear rhenium compounds **5**, ***E*-6(S)**, ***E*-6[PF$_6$]**, ***E*-6[PF$_6$]$_2$** and **7[PF$_6$]$_2$** could be structurally characterized. The structures of **5**, ***E*-6[PF$_6$]** and ***E*-6[PF$_6$]$_2$** are described in the ESI.† ORTEP like drawings of ***E*-6(S)** and **7[PF$_6$]$_2$** are displayed in Fig. 1 and selected bond lengths and angles of **5**, ***E*-6(S)**, ***E*-6[PF$_6$]**, ***E*-6[PF$_6$]$_2$** and **7[PF$_6$]$_2$** are summarized in Table 1.

The Re1–C1 bond of *trans*-[(Me$_3$SiC≡C)(PMe$_3$)$_4$Re≡C–CH$_2$–CH$_2$–C≡Re(PMe$_3$)$_4$(C≡CSiMe$_3$)][PF$_6$]$_2$ (**5**) (see the ESI†) showed a Re≡C distance of 1.7834(19) Å, slightly longer than the expected range (1.75–1.72 Å) of the sum of covalent radii of the Re≡C(sp) unit. The C1–C2 and C2–C2′ bond lengths of 1.491(3) Å and 1.513(4) Å fall into the range of C(sp)–C(sp^3) and C(sp^3)–C(sp^3) single bonds.

The structures of ***E*-6(S)**, ***E*-6[PF$_6$]**, and ***E*-6[PF$_6$]$_2$** all revealed *E*-configurations of the bridging units. The C_4H_2 bridges of ***E*-6(S)**, ***E*-6[PF$_6$]**, and ***E*-6[PF$_6$]$_2$** show features of delocalized systems, for instance the Re1–C1 bond distance of ***E*-6** (1.904(2) Å) is significantly shorter than the Re=C distance of 2.046(8) Å of the vinylidene complex *trans*-[ReCl(=C=CHPh)(dppe)$_2$].[34] Upon stepwise oxidation to ***E*-6[PF$_6$]** and ***E*-6[PF$_6$]$_2$** the Re–C1 bonds shorten to 1.851(6) Å and to 1.805(5) Å, respectively, indicating gradual adoption of a triple bond character. The C1–C2 bond length 1.337(3) Å of ***E*-6(S)** lies within the C=C double bond range 1.33–1.38 Å, while the same bonds of ***E*-6[PF$_6$]** and ***E*-6[PF$_6$]$_2$** with 1.414(7) Å and 1.375(8) Å, respectively, elongate and move closer in distance toward C(sp)–C(sp^2) single bonds averaging at 1.43 Å.[35] The C2–C2′ distance of 1.469(4) Å of ***E*-6(S)** is in agreement with a single bond between two sp^2 hybridized carbon atoms,[35] while the same bonds in ***E*-6[PF$_6$]** and ***E*-6[PF$_6$]$_2$** are 1.388(10) Å and 1.331(10) Å, respectively, within the range of C=C double bonds 1.33–1.38 Å. In conclusion, according to Table 1, upon oxidation of the neutral complex ***E*-6(S)** to the dicationic complex ***E*-6[PF$_6$]$_2$**, the Re1–C1 distances gradually shorten coinciding with a change in the bond order from Re=C to Re≡C. The C1–C2 distances gradually lengthen from a C=C double to a C–C single bond, while the C2–C2′ distances shorten from a C–C single bond to a C=C double bond. The Re⋯Re distances gradually decrease from the neutral complex ***E*-6(S)** to the corresponding dicationic complex ***E*-6[PF$_6$]$_2$**. All these observations clearly indicate that the oxidation of ***E*-6(S)** causes the sp^2 C_4H_2 linkage to transform from a bisvinylidene to an ethylenylidene biscarbyne structure (Scheme 1). These data coincide with the results of the NMR experiments that upon oxidation of ***E*-6(S)** to ***E*-6[PF$_6$]$_2$**, the resonances of C_α showed an up-field shift, while those of C_β and H moved downfield.

The Re1–C1 bond distance of **7[PF$_6$]$_2$** of 1.814(4) Å is close to the corresponding bond length of ***E*-6[PF$_6$]$_2$** of 1.805(4) Å. Taken together with the short C2–C2′ bond of 1.197(8) Å, this provides clear evidence for an alkynediyl biscarbyne canonical form of the bridge in **7[PF$_6$]$_2$**.

The phosphine ligands of the ReP_4 subunits of all complexes **5**, ***E*-6(S)**, ***E*-6[PF$_6$]**, ***E*-6[PF$_6$]$_2$**, and **7[PF$_6$]$_2$** may not just play the role of ancillary ligands being 'innocent' bystanders, but, in most cases, seem to actively contribute to stabilizing the respective valence structure of the C_4H_y bridge (see section III). We first note that the ReP_4 'equatorial' arrangements as subunits of pseudo-octahedral complexes are not planar, but are significantly distorted towards C_{2v} symmetry with one *trans* P–Re–P angle significantly smaller than 180° (about 156°) and bent back toward the acetylide ligands and with the other *trans* P–Re–P angle being between 166° and 170° and bent towards the C_4H_2 or C_4 bridge as schematically sketched in Scheme 9.

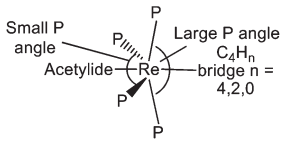

Scheme 9 Sketch of *trans* phosphine angle distortions of the ReP_4 'equatorial' plane toward a C_{2v} local symmetry for complexes **5**, ***E*-6(S)**, ***E*-6[PF$_6$]**, ***E*-6[PF$_6$]$_2$**, and **7[PF$_6$]$_2$**.

As was already discussed, the structural and compositional changes of the bridges of **5**, ***E*-6(S)**, ***E*-6[PF$_6$]**, ***E*-6[PF$_6$]$_2$**, and **7[PF$_6$]$_2$** are also reflected in the $^{13}C\{^1H\}$ NMR spectra. This lets us conclude that the carbon framework in the alkyne biscarbyne complex **7[PF$_6$]$_2$** is more electron-rich than that in the ethylenylidene biscarbyne complex **6[PF$_6$]$_2$**. The C1–C2 bond length in **7[PF$_6$]$_2$** of 1.363(5) Å is slightly shorter than a typical C(sp)–C(sp) single bond (1.377 Å), but close to the corresponding C1–C2 bond distance in the tungsten complex [I(dppe)$_2$W≡C–C≡C–C≡W(dppe)$_2$I] with a bond length of 1.34(1) Å.[13c] The C2–C2′ distance of 1.197(8) Å is within the C≡C triple bond range (1.18–1.20 Å). Therefore the structure of **7[PF$_6$]$_2$** consists of two symmetrically arranged [*trans*-X(PMe$_3$)$_4$Re] fragments linked by a C_4 system resembling a canonical alkynediyl biscarbynic structure. Owing to the practically linear structure of the Re–C_4H_n–Re entity, the Re···Re distance in **7[PF$_6$]$_2$** of 7.536 Å is longer than the corresponding distance in ***E*-6[PF$_6$]$_2$**. The alkynediyl biscarbynic structure of the C_4 chain in **7[PF$_6$]$_2$** differs from the all-cumulenic butatrienediylidene one in the dicationic dinuclear rhenium complex [(Cp*)(NO)(PPh$_3$)ReC$_4$Re(PPh$_3$)(NO)(Cp*)][PF$_6$]$_2$ reported by Gladysz and coworkers. The results clearly reflect the influence of the different electron counts and redox properties of the terminal metal entities and of the ancillary ligand frameworks eliciting different valence structures of the [Re]–C_4–[Re] linkages.

III. DFT calculations on the electronic states of *E*-6 and 7 revealing redox non-innocent structures

A closer insight into the electronic structures of the complexes ***E*-6** and **7** was expected from a thorough DFT analysis based on an appropriate methodological approach to enable the description and proper evaluation of open and closed shell electronic configurations (for details, see the ESI†).

IIIa. Qualitative orbital representation of the pseudo-octahedral [(acetylide)(PMe$_3$)$_4$Re(bridge)] complex unit

The ligand field picture of the pseudo-octahedral [(acetylide)(PMe$_3$)$_4$Re(bridge)] complex is expected to reveal three non-bonding d-orbitals at the rhenium center. According to their parent octahedral coordination geometries (O_h symmetry) these occupied orbitals are denoted as "t_{2g}". Due to the observed apparently sterically induced lowering of the symmetry of the ReP$_4$ units to C_{2v}, splitting of the "t_{2g}" orbitals into two π-type d/p hybridized donor orbitals and one δ-type orbital occurs (Scheme 10).

In the small P angle plane (π_y) the extent of the d/p hybridization is larger and the larger side of the hybrid lobes is directed toward the bridge. The extent of d/p hybridization in the large P angle plane (π_x) is smaller and the larger side of the hybrid lobes is directed away from the bridge. The C_{2v} distortion thus makes the π plane of the smaller P angle plane (π_y) more electron donating to the side of the bridge and the π plane of the larger P angle plane (π_x) less electron donating toward the bridge. The π interactions are thus anisotropic to the bridge side with the consequence that the strongest π orbital interaction results in π anisotropic orbitals of a bridge possessing for instance a π_y acceptor orbital and a π_x donor orbital.[33] This mechanism of an optimum electronic fit seems to be in operation for the complexes ***E*-6(S)**, ***E*-6[PF$_6$]**, ***E*-6[PF$_6$]$_2$** and **7(S)** supporting the binding in certain ReC$_4$H$_2$Re and ReC$_4$Re moieties. For the carbyne complex **5** and for **7[PF$_6$]$_2$** involving a conical Re≡C carbyne interaction the C_{2v} distortion of the ReP$_4$ fragment is anticipated to be primarily of steric origin without additional support from the rhenium–bridge interaction.

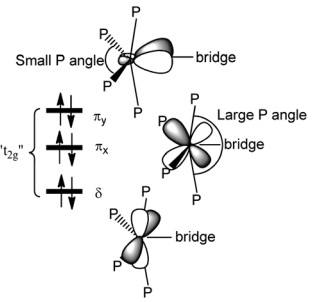

Scheme 10 Qualitative representation of the filled non-bonding d-orbitals ("t_{2g}") of an [(acetylide)(PMe$_3$)$_4$Re(bridge)] unit with two π type orbitals (π_x and π_y) and one δ type orbital.

IIIb. DFT calculations on *trans*-[(Me$_3$SiC≡C)(PMe$_3$)$_4$ReC$_4$H$_2$Re(PMe$_3$)$_4$(C≡CSiMe$_3$)] (*E*-6(S)) and *trans*-[(Me$_3$SiC≡C)(PMe$_3$)$_4$ReC$_4$Re(PMe$_3$)$_4$(C≡CSiMe$_3$)] (7)

We carried out structure optimizations for *trans*-[(Me$_3$SiC≡C)(PMe$_3$)$_4$ReC$_4$H$_2$Re(PMe$_3$)$_4$(C≡CSiMe$_3$)] (***E*-6(S)** and *trans*-[(Me$_3$SiC≡C)(PMe$_3$)$_4$ReC$_4$Re(PMe$_3$)$_4$(C≡CSiMe$_3$)] (**7**) by means of Kohn–Sham DFT (for details, see Computational methodology). If not mentioned otherwise, the BHLYP hybrid functional with 50% Hartree–Fock exchange was employed.[36] As shown for organic mixed-valence compounds,[37] it is important to include a proper amount of the exact exchange, since standard non-hybrid and hybrid exchange–correlation functionals give a too delocalized description.[38]

***trans*-[(Me$_3$SiC≡C)(PMe$_3$)$_4$ReC$_4$H$_2$Re(PMe$_3$)$_4$(C≡CSiMe$_3$)] (*E*-6).** The possible isomers of the neutral molecule ***E*-6** are the diamagnetic geometric isomers ***E*-6(S)** and ***Z*-6(S)** and the open-shell, diradical alternatives ***E*-6(F)** and ***E*-6(A)** (Scheme 1) possessing SOMOs with either anti- or ferromagnetically coupled electrons. Isomers ***Z*-6(F)** and ***Z*-6(A)** were not considered due to the expected very high electronic energies for these molecules and the fact that none of them was experimentally observed.

***E*-6(S)** was calculated to have the lowest electronic energy constituting the ground state of ***E*-6** (Scheme 10). The calculations for the singlet diradical structure ***E*-6(A)** did not converge (the same was found, if the PBE0[39] or B3LYP density

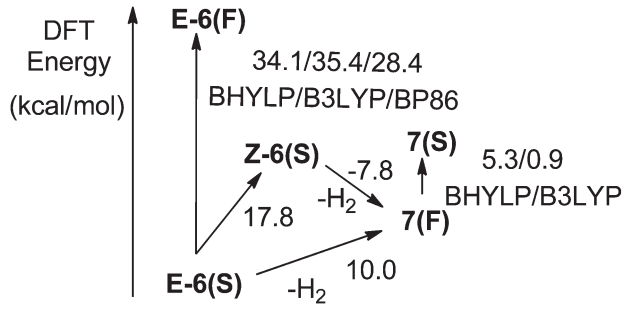

Scheme 11 Scheme of calculated electronic energies for two isomers of ***E*-6** and **7** and their isomerization and dehydrogenation reactions. Energies in kcal mol^{-1} obtained from DFT geometry optimizations applying different exchange–correlation density functionals indicated underneath the energy values.

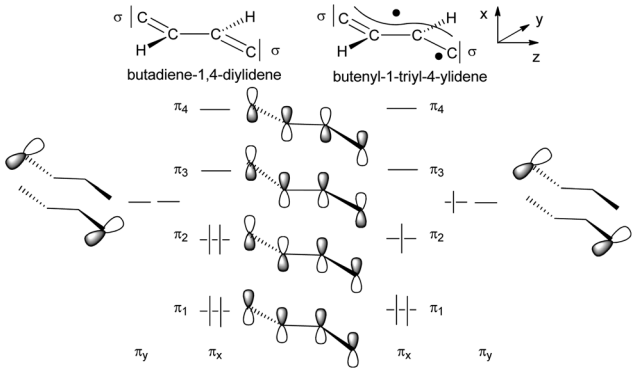

Scheme 12 Schematic MO picture of two electronic states of the C_4H_2 bridge.

functionals[36a,b,40] were used) indicating that this state is perhaps also not of practical relevance. The ***E*-6(F)** state could be optimized with different density functionals (BHLYP/B3LYP/BP86)[36a,41] leading to slightly different electronic energies, but all of these energies were at levels much higher (34.1/35.3/28.4 kcal mol^{-1}) than that of ***E*-6(S)** (Scheme 11). Given the large energy difference ***E*-6(F)** can be considered an electronic excited state of ***E*-6(S)**.

The potential energy surface of ***E*-6(S)** was theoretically explored further by a thermodynamic evaluation calculating first the geometric *Z* isomer ***Z*-6(S)**, which could not be detected in solution. By structural optimizations ***Z*-6(S)** turned out to be 17.8 kcal mol^{-1} higher energy than ***E*-6(S)**. This makes its existence in solution at room temperature very unlikely. One can safely assume that, if formed, it will spontaneously convert to ***E*-6(S)** with a very low barrier. Another possible deactivation pathway is dehydrogenation to **7**. For the thermally stable ***E*-6(S)** the dehydrogenation process is uphill in energy (Scheme 12).

In the following section the electronic structures of ***E*-6(S)** and ***E*-6(F)** are discussed, which will be accomplished by a fragmental view of the molecules dividing the molecules up into the [(acetylide)$(PMe_3)_4$Re] fragment with the π type large and small P angle plane d_{Re} orbitals combined with π orbitals of the different bridge states.

The frontier orbitals of *E*-6(S). The DFT calculations of ***E*-6(S)** as the ground state of ***E*-6**, gave proof of the butadiene-1,4-diylidene canonical form (Scheme 1) as the prevailing MO picture of the bridge. The π orbital system of a butadiene-1,4-diylidene is qualitatively described in Scheme 12.

The qualitative MO picture of the C_4H_2 bridge (Scheme 12) shows two perpendicular π systems denoted as π_x and π_y, which have different electron occupancies for the closed shell or open shell electronic configurations of butadiene-1,4-diylidene and butenyl-1-triyl-4-ylidene. Scheme 11 will be used to identify the bridge contributions of prominent MOs of ***E*-6(S)** and ***E*-6(F)** as they are obtained from the DFT calculations.

The butadiene-1,4-diylidene bridge of ***E*-6(S)** possesses two main components for π-type orbital interactions with the

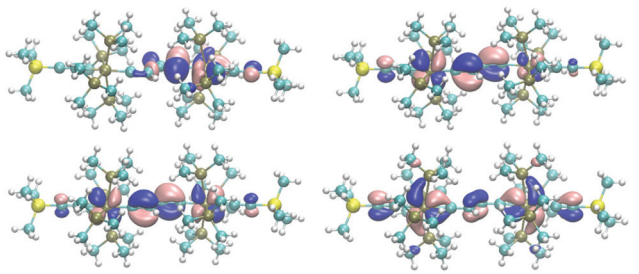

Fig. 2 Top: views of the two SOMOs of ***E*-6(F)** demonstrating for both orbitals relative strong localization on the carbenic (rhenium–carbon)$_{bridge}$ bond (d_{Re}–π_y) (left, HOMO) and the ($\pm d_{Re}(\pi_x)$)–π_2 orbital (right, HOMO–1). Bottom: orbital plots of the HOMO (left) and HOMO–1 (right) of ***E*-6(S)**.

rhenium fragments. First there is a net weak π donor interaction in the π_x plane originating from the interaction with the filled π_2 orbital, which is complemented by the π acceptor interaction with the empty π_3 orbital. Second in the π_y plane the bridge behaves as a strong π acceptor due to the interactions with the empty carbene p orbitals and the d_π orbitals at each rhenium center. The main destabilizing component of the π donor interaction is found in the HOMO of ***E*-6(S)** and can be viewed as the antibonding component $d_{Re}(\pi_x)$–π_2, where π_2 is out-of-phase with the $d_{Re}(\pi_x)$ orbitals (Fig. 2, bottom left). The antibonding $d_{Re}(\pi_x)$–π_2 orbital has as a bonding counterpart $d_{Re}(\pi_x)$+π_2 lying at a quite low energy. Of further significance for the overall orbital description of ***E*-6(S)** is the HOMO–1 (Fig. 2, bottom right), which is composed of the bonding combination of π_3 with the in-phase-combination of $d_{Re}(\pi_x)$ orbitals in the small P angle plane $d_{Re}(\pi_x)$+π_3. The HOMO–1 thus has the effect of a π acceptor interaction counteracting and attenuating partly the effect of π electron donation. The overlay of the electron densities of these π interactions with the mentioned main contributions of the [Re]CC(H)C(H)C[Re] fragment describes well the bridge's C1–C2 and C2–C2′ full and partial double bond characters. The minor influence of HOMO–1 can be recognized by (a slight) elonga-

tion of the C1–C2 and C1′–C2′ bonds of ***E*-6(S)** and a greater influence on the shortening of the C2–C2′ toward a double bond (*cf.* Table 1). Selected calculated structural parameters of ***E*-6(S)** are compiled in Table 1 in comparison with the data obtained from the X-ray diffraction study demonstrating very good agreement in distances and angles.

The frontier orbitals of *E*-6(F). The diradical non-innocent isomer ***E*-6(F)** turns out to be an excited state of ***E*-6(S)**. This excitation of one electron is reflected in the orbitals of the bridge: one electron of π_2 of the butadiene-1,4-diylidene was promoted to a π_y orbital of the butenyl-1-triyl-4-ylidene (Scheme 12). The butenyl-1-triyl-4-ylidene moiety has thus two energetically different SOMOs. The SOMO at the highest energy is localized on one of the carbenic p orbitals. Upon interaction with the (acetylide)$Re(PMe_3)_4$ fragment this electron resides at one rhenium center in a strongly antibonding orbital *via* the interaction of π_y of the bridge and the $d_{Re}(\pi_y)$ orbital in the small P angle plane ($d_{Re}(\pi_y)$–π_y) (Fig. 2, top left) weakening the (rhenium–carbon) bridge bond and forming the high energy SOMO of ***E*-6(F)**. Together with the bonding orbital $d_{Re}(\pi_y)$+π_y, the counterpart of $d_{Re}(\pi_y)$–π_y, a three-electron π bond with a π bond order of $\frac{1}{2}$ results. The other SOMO of ***E*-6(F)** at a lower energy (Fig. 2, top right) is mainly localized over one [Re]CCHCHC unit and is composed of an out-of-phase combination of the $d_{Re}(\pi_x)$ orbital (Scheme 11) and the singly occupied π_2 orbital of the butenyl-1-triyl-4-ylidene system $d_{Re}(\pi_x)$–π_2). This antibonding ($\pm d_{Re}(\pi_2)$)–π_2 orbital has a bonding counterpart 2($\pm d_{Re}$)+π_2 summing up to a rhenium–carbon three-electron π bond and a total π bond order of $\frac{1}{2}$. The bonding balance of each of the SOMOs is thus based on two three-electron-interactions of the bond order $\frac{1}{2}$, one at each rhenium center. It may be worth mentioning that none of the SOMOs of ***E*-6(F)** provides full 'through-bridge' electronic interaction between the rhenium centers (Fig. 2, top). Actually removing the two antibonding SOMO electrons from the ***E*-6(F)** molecule makes the rhenium centers electron precise allowing for a strong carbynic ethylenylidene-1,4-ditriyl bridge structure ([Re]≡C–CH=CH–C≡[Re]).

***trans*-[($Me_3SiC{\equiv}C$)(PMe_3)$_4$ReC_4Re(PMe_3)$_4$($C{\equiv}CSiMe_3$)] (7).** In contrast to complex ***E*-6**, where the diradical structure ***E*-6(F)** is energetically too high to be considered as a ground state or close to it, DFT calculations on **7** suggest that the diradical structure of **7(F)** is slightly lower in energy by 5.3/0.9 kcal mol^{-1} than the singlet state **7(S)** using the BHYLP/B3LYP density functional (Scheme 11). Given the relatively high confidence intervals for the electronic energies of the hybrid type DFT calculations, we have to consider both configurations energetically close so that they may co-exist at room temperature in solution. It is also possible that **7(S)** is even of a lower energy than **7(F)**. The calculated main structural parameters of **7(S)** and **7(F)** are compiled in Table 1 and according to these both have very similar structures. The slightly longer Re–C bond lengths of **7(F)** may reflect a somewhat higher degree of the antibonding character of the metal–carbon bonds. Despite these small structural differences, these molecules may constitute examples of bond length isomerism.[21e,42]

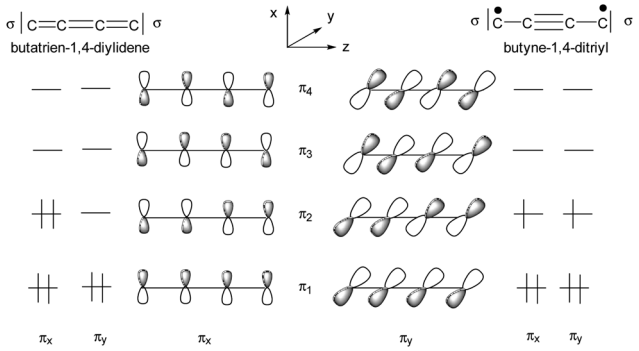

Scheme 13 Schematic MO picture of two electronic states of the C_4 bridge.

Orbitals and electronic states of the non-innocent isomers 7(F) and 7(S). The qualitative MO picture of the C_4 bridge reveals that terminal σ orbitals and two mutually perpendicular and degenerate π systems, π_x and π_y, may exhibit two different electron occupancies (Scheme 13), namely the closed or open shell configurations of butatriene-1,4-di(ylidene) and butyne-1,4-di(triyl), respectively. The π_x and π_y orbitals of the C_4 system are occupied by a total of 6 electrons (Scheme 13). Arranging these 6 electrons in pairs as in the spin-paired butatriene-1,4-di(ylidene) configuration an asymmetric distribution of the π planes results with 4 and 2 electrons for π_x and π_y. For the butyne-1,4-di(triyl) moiety Scheme 13 describes the equal distribution of six π electrons of the bridge generating two singly occupied SOMOs corresponding to the degenerate, bonding π_2 orbitals in the orthogonal π_x and π_y orbital planes.

Given these basic orbital descriptions of the bridge we continue to first analyze the compositions of the **7(F)** orbitals by attachment of (acetylide)$Re(PMe_3)_4$ fragments on both sides of the butyne-1,4-di(triyl) bridge. The two π_2 SOMO orbitals interact with the filled π_x and π_y orbitals of the rhenium centers and get transformed into SOMOs of **7(F)** forming two half-filled π donor interactions antibonding with respect to the rhenium–carbon interactions of the $d_{Re}(\pi_x,\pi_y)$–π_2 orbital character. Fig. 3 (top) shows the orbital drawing of one of the – on the DFT basis – nearly degenerate SOMOs. The bonding orbital counterparts of the SOMOs are the $d_{Re}(\pi_x,\pi_y)$+π_2 orbitals, occupied by two electrons, which are located at quite low electronic energies. These two 3-electron π donor interactions amount to a total binding balance of the rhenium–carbon π bond order of $\frac{1}{2}$ each. In each π plane (π_x and π_y) there is however an additional π acceptor interaction involving π_3 of the π_x and π_y ($d_{Re}(\pi_x,\pi_y)$+π_3), which could in the best case reach a maximum bond order of 1 at each rhenium center. Counting in addition the two σ electron pairs of the bridge contributing a bond order of 1 to the $(Re–carbon)_{bridge}$ bond a total bond order of $2\frac{1}{2}$ would result. Since the SOMOs of **7(F)** bear the bonding character of π_2 of the bridge, these lie at lower electronic energies than the SOMOs of ***E*-6(F)**, which have more antibonding character. The relatively low energy and the extensive delocalization of the SOMOs of **7(F)** is also the cause for

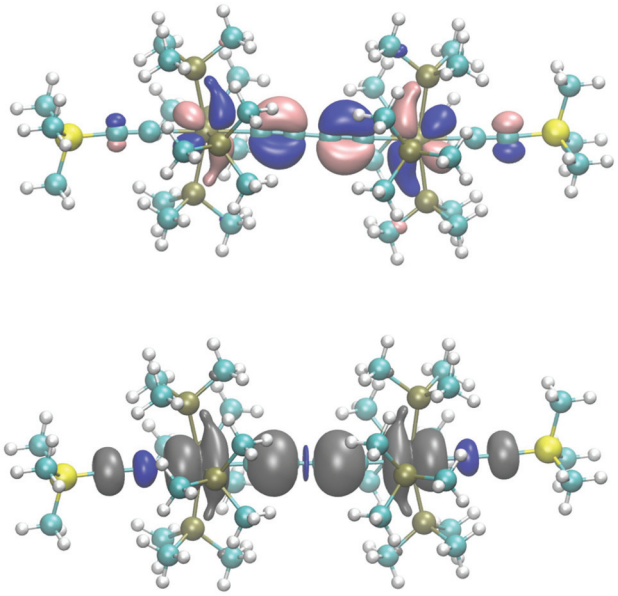

Fig. 3 Top: orbital representation of one of the perpendicular SOMO π orbitals of **7(F)**. Bottom: plot of the calculated spin density of **7(F)** (B3LYP/def2-TZVP/COSMO; grey: isosurface at 0.002 e $Bohr^{-3}$, blue; isosurface at −0.002 e $Bohr^{-3}$).

the competitive total electronic energies of isomeric **7(F)** and **7(S)** (*vide infra*).

In line with the overlaid shapes of the SOMOs of **7(F)**, the spin density (spin-down (β) electronic densities) in Fig. 3 is conical along the main axis of the molecule and to a large extent positive on the rhenium centers, the carbon atoms of the bridge, and the acetylenic β atoms. A significant excess of the β spin density is also obtained on the acetylenic α atoms presumably *via* a spin polarization mechanism.[43]

As shown in Scheme 12 the butatriene-1,4-di(ylidene) electron occupancy of six π electrons of a C_4 bridge would be unequal with respect to the π_x and π_y planes, which in the case of **7(S)**, causes anisotropy in the π interactions with the rhenium centers. Since the π_x and π_y planes of the rhenium centers are different in p,d hybridization and energy, they are anisotropic in character (Schemes 8 and 9). This leads to cooperativity in the interactions with the likewise anisotropic π orbitals of the bridge (the stronger π donor plane of the rhenium center interacts with the stronger π acceptor plane of the bridge and *vice versa*). The HOMO (π_x plane), HOMO−1 (π_y plane) and the second π acceptor interaction (π_y plane) of **7(S)** (Fig. 4, bottom) indeed reflect the highly anisotropic character of the ReC_4Re π interactions consisting thus mainly of one π donor and two π acceptor interactions with the rhenium center.

The HOMO represents an antibonding interaction between the $d_{Re}(\pi_x)$ orbital of the large P angle plane (Scheme 9) with π_2 of the bridge. Due to the small bending toward the bridge orbital overlap is reduced on the bridge side, thus decreasing the repulsive character of the 4-electron interaction of $d_{Re}(\pi_x)$ with π_2 of the bridge (HOMO, Fig. 4, top).[33] The π_y MOs of the bridge – coplanar with the stronger π_y donor orbitals of the

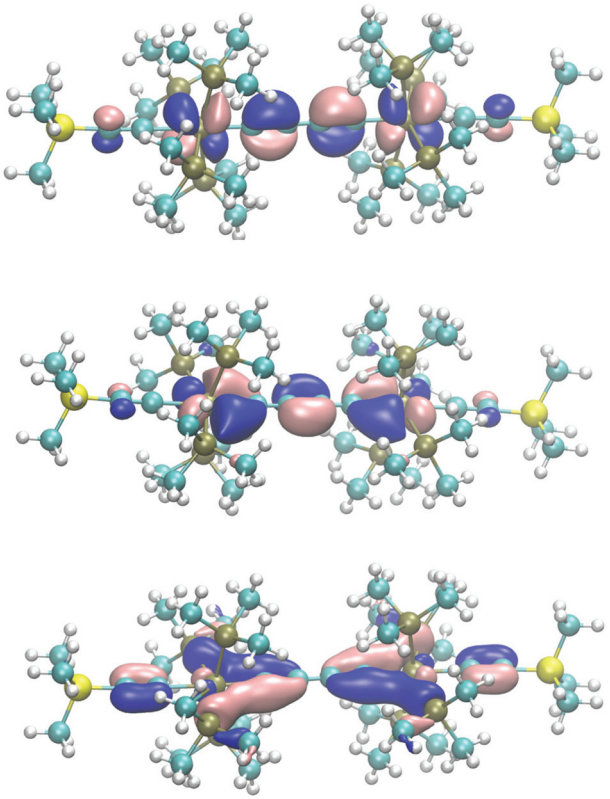

Fig. 4 Three orbital plots selected from the orbitals of **7(S)** in qualitative order of their energies. Top: HOMO, middle: first π acceptor interaction of **7(S)** (HOMO−1, π_y plane) bottom: plot of the second π_y acceptor orbital at low electronic energy.

rhenium fragment – are prone to very strong π acceptor interactions engaging even two $d_{Re}(\pi_y)+(\pi_2,\pi_3)$ π-type interactions. The $d_{Re}(\pi_y)$ orbitals at each rhenium center of **7(S)** form an in-phase and an out-of-phase orbital combination, which at one time each interacts in a bonding fashion with π_3 (HOMO−1, middle of Fig. 4) or with π_2 of the bridge to establish the second π acceptor orbital lying at low electronic energies (Fig. 4, bottom). In a localized bonding picture these two π bonding orbitals would account for one π bond at each rhenium center and together with the σ bonds the Re=C double bond character results.

IV. Electrochemical and spectroscopic studies of *E*-6(S) and 7

IVa. Cyclic voltammetry (CV) studies of the dinuclear rhenium complexes *E*-6(S), *E*-6$[PF_6]_2$ and 7$[PF_6]_2$

Voltammograms of *E*-6$[PF_6]_2$ (Fig. 2a) recorded in THF displayed two reversible waves at $E_{1/2}$ = −1.292 V and $E_{1/2}$ = −1.749 V. The electrochemical and structural data in concert support a stepwise reduction of *E*-6$[PF_6]_2$. This is accompanied by an electronic re-adjustment of the C_4H_2 linkage from an ethylene biscarbyne to a bis(vinylidene) structure revealing that the

Table 2 Electrochemical data for **6**, **6**[PF_6]$_2$ and **7**[PF_6]$_2$ and for some dinuclear manganese and rhenium complexes, *E vs.* $Fc^{0/+}$

Complexes	Couple 1 $E_{1/2}$ (V)	Couple 2 $E_{1/2}$ (V)	ΔE (V)	K_c	Ref.
[($Me_3SiC{\equiv}C$)(PMe_3)$_4$Re≡C–CH=CH–C≡Re(PMe_3)$_4$($Me_3SiC{\equiv}C$)][PF_6]$_2$ (***E*-6**[PF_6]$_2$)	−1.292	−1.749	0.457	7.1×10^7	Present work
[(MeC_5H_4)(depe)Mn≡C–CH=CH–C≡Mn(depe)(MeC_5H_4)][PF_6]$_2$	−0.820	−1.386	0.576	6.6×10^9	23*d*
[(MeC_5H_4)(dmpe)Mn–C≡C–Mn(dmpe)(MeC_5H_4)][PF_6]$_2$	−0.847	−1.835	0.988	8.6×10^{16}	23*d*
[($Me_3SiC{\equiv}C$)(PMe_3)4Re≡C–C≡C–C≡Re(PMe_3)$_4$($Me_3SiC{\equiv}C$)]$_2$[PF_6]$_2$ (**7**[PF_6]$_2$)	−1.164	−1.668	0.504	4.7×10^8	Present work
[(Cp*)(NO)(PPh_3)Re–C≡C–C≡C–Re(PPh_3)(NO)(Cp*)]	0.06	0.59	0.53	1.1×10^9	10*a*

redox processes are to a great extent bridge-centered as is also mandated by the HOMO of ***E*-6**[PF_6]$_2$ as shown in Fig. 2. The potential difference $\Delta E_{1/2}$ between the two redox waves of 0.457 V results in a K_c value of 7.1×10^7. Cyclic voltammetry measurements of ***E*-6(S)** gave identical results apart from the fact that the forward peaks were now anodic instead of cathodic. In comparison with the manganese analog [(MeC_5H_4)(dmpe)Mn≡C–CH=CH–C≡Mn(dmpe)(MeC_5H_4)][PF_6]$_2$, the values of the two redox couples of ***E*-6**[PF_6]$_2$ are more negative and the K_c value is smaller (Table 2). In accordance with the CV study, neutral ***E*-6** is very easy to oxidize (Fig. 5).

The CV of *trans*-[($Me_3SiC{\equiv}C$)(PMe_3)$_4$ReC_4Re(PMe_3)$_4$(C≡C-$SiMe_3$)][PF_6]$_2$ (**7**[PF_6]$_2$) in THF showed four separate waves with high degrees of chemical reversibility corresponding to four consecutive reductions from $[7]^{2+} \rightarrow [7]^{+} \rightarrow [7] \rightarrow [7]^{-} \rightarrow [7]^{2-}$. The potential difference $\Delta E_{1/2}$ between the first redox waves of **7**[PF_6]$_2$ is 0.504 V resulting in a K_c value of 4.7×10^8 with **7**[PF_6] as an in principle isolable intermediate redox state as also revealed in the spectro-electrochemical studies. However, attempts to prepare **7**[PF_6] were unsuccessful. The third and fourth redox processes have very negative potentials, which make the corresponding reduced species $[7]^{-}$ and $[7]^{2-}$ difficult to prepare by chemical methods. For $[7]^{-}$ and $[7]^{2-}$ we have to assume bridge-centered reduction steps. The $\Delta E_{1/2}$ values of the complexes **6**[PF_6]$_2$ (0.475 V) and **7**[PF_6]$_2$ (0.504 V) are very close. The only difference in these complexes are the bridges, therefore one might conclude that the strengths of electronic communication through the C_4H_2 and the C_4 bridges are very similar.

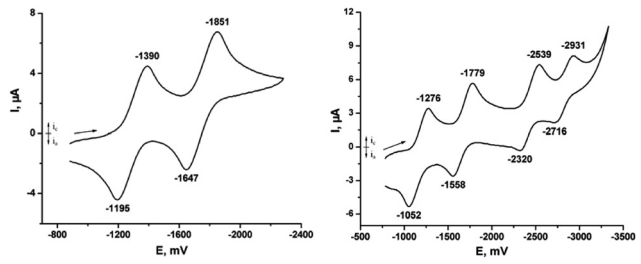

Fig. 5 Cyclic voltammogram of ***E*-6**[PF_6]$_2$ in 0.1 M THF solution of [*n*-Bu_4N][PF_6], Au electrode; *E vs.* $Fc^{0/+}$; scan rate = 100 mV s^{-1}; 20 °C. CV of **7**[PF_6]$_2$ in 0.1 M THF solution of [*n*Bu_4N][PF_6], Au electrode; *E vs.* $Fc^{0/+}$; scan rate = 100 mV s^{-1}; 20 °C.

IVb. NIR evidence for through-bridge electronic interaction in *E*-6(S), *E*-6[PF_6] and *E*-6[PF_6]$_2$

To further assess the extent of the electronic interaction between the two redox-active rhenium centers of ***E*-6(S)**, ***E*-6**[PF_6] and ***E*-6**[PF_6]$_2$, the UV-vis spectra of ***E*-6(S)**, ***E*-6**[PF_6] and ***E*-6**[PF_6]$_2$ were examined (Fig. 6). Due to limited solubility and stability in other solvents, the neutral complexes could be studied in THF only and the examination of a solvent effect of the MV complexes could not be performed. The UV-vis spectral data and IVCT absorption data for the MV complexes are listed in Tables 2 and S3.†

The UV-vis spectra of all complexes ***E*-6(S)**, ***E*-6**[PF_6], and ***E*-6**[PF_6]$_2$ show intense absorption bands in the visible and ultraviolet region, which can be attributed to a metal-to-ligand charge transfer (MLCT) transition (Fig. 6 and Table S3 in the ESI†). In the visible and near-infrared region an additional absorption band is observed at approximately 897 nm (ε is about 1.90×10^4 M^{-1} cm^{-1}) with a notable shoulder at ~800 nm for the MV complex ***E*-6**[PF_6]. There are no counterparts in the spectra of the corresponding neutral complex ***E*-6(S)** and the dicationic complex ***E*-6**[PF_6]$_2$, so that they may be identified as intervalence charge transfer (IVCT) bands. Observations of multiple IVCT bands have been reported previously for the MV complexes {[(MeC_5H_4)(dmpe)Mn]$_2$(≡C–CPh=CPh–C≡)}$^+$,[24b] {[(η^5-C_5Me_5)(NO)(PPh_3)Re]$_2$(μ-C≡C–C≡C)}$^+$,[10a] {[(C_5Me_5)(dppm)Ru]$_2$(μ-C≡C–C≡C)}$^+$ [30] and {[(C_5Me_5)(dppm)-Fe]$_2$(μ-C≡C–X–C≡C)}$^+$ (X = 2,5-C_4H_2S, –C_4–).[44] One explanation considered is spin–orbit coupling, which is of particular relevance in third-row transition metals.[45] An alternative assignment is that one absorption is a LMCT transition, and the other a MLCT transition.[10a,24b,30,44,46] Considering the strongly metal–ligand delocalized nature of the frontier MOs, the underlying transitions may be best viewed as π → π* type transitions within a conjugated open-shell metal–organic π-system with only a limited amount of charge transfer between the individual constituents.[30,47] On the premise that the observed absorptions can be viewed as IVCT transitions, a Gaussian analysis of the IVCT absorption band of the MV complex was performed in order to calculate the electronic coupling energy H_{ab}.[44,46] The spectrum of the mixed valence complex ***E*-6**[PF_6] can be deconvoluted into three Gaussian bands A, B, and C (ESI†), where band B is the major component, and with a tail of the MLCT band observed in the visible and ultraviolet regions. Spectral data extracted from the IVCT band shape analyses are summarized in Table S3 (ESI).†

Table 3 UV-vis-NIR spectral data for complexes ***E*-6(S)**, ***E*-6[PF$_6$]**, and ***E*-6[PF$_6$]$_2$**

Complex	λ_{max} (nm)	ν_{max} (cm^{-1})	ε_{max} (M^{-1} cm^{-1})
***E*-6(S)**	390	2.56×10^4	4.04×10^4
***E*-6[PF$_6$]**	457	2.19×10^4	5.02×10^4
	897	1.14×10^4	1.90×10^4
***E*-6[PF$_6$]$_2$**	460	2.17×10^4	3.30×10^4

The observed bandwidths of the three bands at half height ($\Delta_{1/2}$) are narrower than those predicted from the equation $\Delta\nu_{1/2}(\text{cm}^{-1}) = (2310 \cdot \nu_{max})^{1/2}$,[7a,48] which is in agreement with a class III character for the MV complex. In addition, the delocalization parameters Γ as calculated from the equation $\Gamma = 1 - \Delta\nu_{1/2}/(2310\nu_{max})^{1/2}$,[7a,49] are larger than (A, B) or close to (C) 0.5 for all bands. Based on the CV and NIR spectroscopic data, the MV complex ***E*-6[PF$_6$]** can be described as a class III MV compound with the odd electron fully delocalized over the Re_2C_4 core. Based on the values of Table 3 electronic coupling energies H_{ab}^{III} for band A, band B, and band C of ***E*-6[PF$_6$]** are 5.43×10^3 cm^{-1}, 6.10×10^3 cm^{-1}, and 7.24×10^3 cm^{-1}, respectively.

EPR studies and magnetic measurements. EPR measurements on the paramagnetic MV complex ***E*-6[PF$_6$]** (Fig. 7a) indicated that ***E*-6[PF$_6$]** is EPR-silent at room temperature. But at 8 K a broad signal of reasonable intensity is observed with unresolvable hyperfine interactions and a g factor of 1.890. The EPR features are consistent with the notion of a metal-perturbed organic spin. Metal contributions to the SOMO can be inferred from the large deviation of the g value from the free-electron value $g_e = 2.0023$ and the EPR silence at higher temperatures. Both may be related to spin–orbit coupling induced by the comparatively large SOC of Re(II/III) of the order of 2100 to 2500 cm^{-1}.[50] On the other hand, more significant rhenium contributions to the overall spin density should give rise to a sextet (in the case of a valence-localized description) or an undecet (in the case of a valence-delocalized situation of class III) splitting due to hyperfine interactions to ^{185}Re and ^{187}Re nuclei. Particularly instructive examples are provided by the organometallic half-sandwich Re complexes [Cp*Re(NO)(PPh$_3$)(CH$_3$)]$^+$, [Cp*Re(NO)(PPh$_3$)(μ-C≡C–)Pd(PEt$_3$)$_2$Cl]$^+$ and [{Cp*Re(NO)(PPh$_3$)(μ-C≡C–)}$_2$-Pd(PEt$_3$)$_2$]$^+$ with g = 2.110–2.121, $A^{185/187}$Re = 190 G) and [{Cp*Re(NO)(PPh$_3$)}$_2$(μ-C≡C–C≡C)]$^+$ (g = 2.018, $A^{185/187}$Re = 98 G).[51] The latter compound was reported to have about equal metal/C_4 ligand contributions to the SOMO (*i.e. ca.* 25% of the total spin density on each Re, atom).[52] Even in the case of the heterobimetallic [{Cp*Re(NO)(PPh$_3$)}(μ-C≡C–C≡C){Fe(dppe)Cp*}]$^+$, where the rhenium contribution to the overall spin density is reduced to *ca.* 17%, Re hyperfine interactions of 48 G were readily discerned.[11b] This all argues for an even lower metal/higher bridge contribution to the SOMO of ***E*-6[PF$_6$]**. On the other hand, the non-observability of Re hyperfine interactions does not allow us to draw any conclusion on the extent of spin delocalization within the [Re–C_4H_2–Re]$^+$ array.

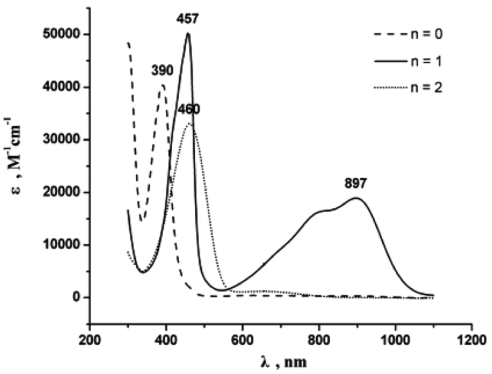

Fig. 6 UV-vis spectra of [***E*-6]$^{n+}$** (n = 0 in THF; n = 1 and n = 2 in CH_3CN, ambient temperature, 5×10^{-5} M).

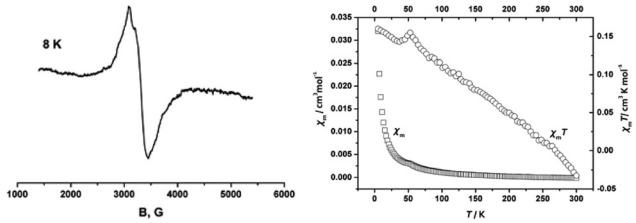

Fig. 7 (a) EPR spectrum of ***E*-6[PF$_6$]** at 8 K in CH_3CN glass; (b) plots of χ_m and χ_mT *vs.* T for ***E*-6[PF$_6$]**.

Variable-temperature magnetic susceptibility measurements were carried out in the temperature range from 5 K to 300 K. The magnetic properties are presented in the form of χ_m and χ_mT *vs.* T plots in Fig. 6b. The MV complex ***E*-6[PF$_6$]** showed typical paramagnetic behavior with the magnetic susceptibility χ_m dropping abruptly from 5 K to 50 K then gradually and the χ_mT value decreasing from 5 K to 300 K. This is a manifestation of the paramagnetism expected from the odd electron in this molecule.[23c]

IVc. Spectro-electrochemical studies on 7[PF$_6$]$_2$

The high chemical reactivity of the reduced forms of complex **7[PF$_6$]$_2$** prevented their isolation as pure compounds. In order to characterize them by IR- and UV-Vis-NIR-spectroscopy we resorted to their generation *in situ* by means of spectro-electrochemistry. Inside an OTTLE (optically transparent thin layer electrolysis) cell three consecutive reductions of **7[PF$_6$]$_2$** could be followed. Just like in the solid state, **7[PF$_6$]$_2$** only showed a weak ν(C≡C) stretching vibration at 2018 cm^{-1} in the THF/NBu_4PF_6 electrolyte. Upon reduction to **[7]$^+$** species the original ν(C≡C) band was replaced by a much stronger absorption at 1992 cm^{-1} and a much weaker one at 1612 cm^{-1}. During the second reduction to the neutral complex **7** the former ν(C≡C) band gave way to an even stronger absorption at 1957 cm^{-1}, while the band at 1612 cm^{-1} was replaced by a stronger one at 1738 cm^{-1} (Fig. 8). Both these processes were fully reversible as ascertained by the presence of clean isosbestic points and

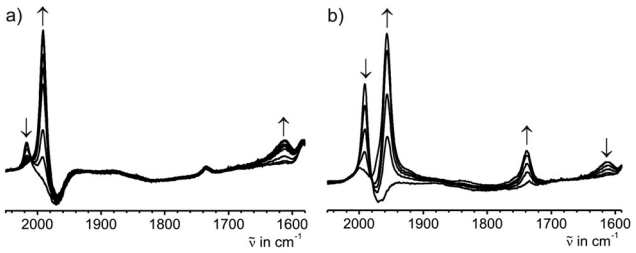

Fig. 8 IR spectroscopic changes during (a) the first and (b) the second reduction of complex $\mathbf{7[PF_6]_2}$ in THF/NBu_4PF_6 at r.t.

full recovery of the original spectrum of $\mathbf{7[PF_6]_2}$ upon exhaustive back electrolysis at a potential sufficiently positive of the $[7]^+/[7]$ and $[7]^+/[7]^{2+}$ redox waves. Identical results were obtained using the 1,2-$C_2H_4Cl_2$/NBu_4PF_6 electrolyte ($[7]^{2+}$: ν(C≡C) = 2016 cm^{-1}; $[7]^+$: ν(C≡C) = 1991 cm^{-1}, $\nu(C_4)$ = 1615 cm^{-1}; **7**: ν(C≡C) = 1958 cm^{-1}, $\nu(C_4)$ = 1738 cm^{-1}). Low energies of ν(CC) stretching bands are not without precedence in C_4-bridged dimetal complexes and are indicative of the cumulenic character of the all-carbon bridge as in **7(S)** (Scheme 6).[11a,23b,f,53] Of note is the rather strong shift of the ν(C≡C) bands assigned to the terminal alkynyl ligands upon stepwise reduction. It is much stronger than in comparable C_4-bridged dimanganese complexes (2026 → 2016 → 2010 cm^{-1}).[23b,f,24a] This points to significant contributions of the terminal alkynyl ligands to the HOMO of $[7]^{2+}$ and the SOMO of $[7]^+$ and hence an enhanced delocalization of the charge onto the terminal alkynyl ligands for the heavier congener.

Attempts to further reduce **7** to $[7]^-$ resulted in a sequence of two consecutive electron transfers and subsequent protonation steps to ultimately yield complex ***E*-6**. This is clearly seen from the growth of ν(C≡C) and ν(C=C) bands at 1972 and 1545 cm^{-1} during this process. These bands are virtually identical to those of pristine solid ***E*-6**. Furthermore, stepwise re-oxidation of the exhaustively reduced solution first gave a ν(C≡C) band at 1999 cm^{-1} and, after the final re-oxidation step, a band at 2022 cm^{-1} in agreement with the ATR data of complexes $\mathbf{\textit{E}\text{-}6[PF]_6}$ and $\mathbf{\textit{E}\text{-}6[PF_6]_2}$. When solutions of $\mathbf{7[PF_6]}$ were on partially electrolyzed at potentials negative of the $\mathbf{7}/[7]^-$ wave the spectroscopic features of species **6** and **7** were detected without any detectable intermediate $[7]^-$ (Fig. 9a). Stepwise reoxidation of such incompletely reduced solutions first produced mixtures of complexes $\mathbf{7[PF_6]}$ and $\mathbf{\textit{E}\text{-}6[PF_6]}$ and then of $\mathbf{\textit{E}\text{-}6[PF_6]_2}$ and $\mathbf{7[PF_6]_2}$ (Fig. 9b and c).

In situ reduction of $\mathbf{7[PF_6]_2}$ under UV/Vis/NIR monitoring also occurred in two well-resolved steps to first produce the radical cation $[7]^+$ and then neutral **7**, again with clean isosbestic points for each individual step (Fig. 10). During the first reduction, the prominent near UV band of $[7]^{2+}$ peaking at 376 nm sharpened and red-shifted into the visible range to produce an intense peak at 409 nm, while a plateau-like absorption of $[7]^{2+}$ with peak positions at 510 and 570 nm develops into a considerably more richly structured absorption

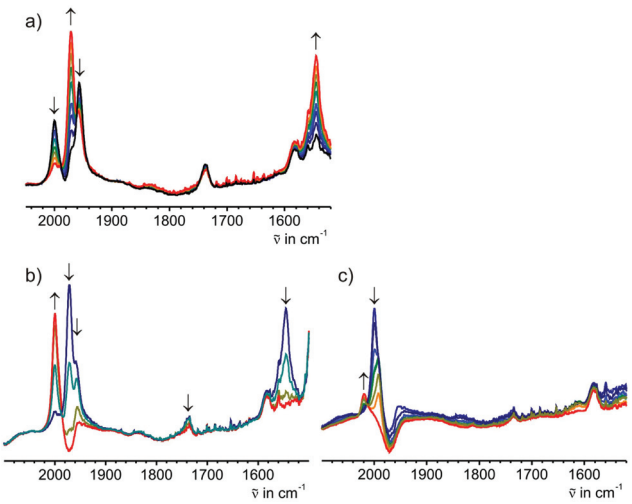

Fig. 9 (a) IR spectroscopic changes upon reduction of complex $\mathbf{7[PF_6]}$ at negative potentials for the $\mathbf{7}/[7]^-$ wave showing the intermediate growth of the C≡C band of **7** at 1955 cm^{-1} and the accompanying growth of the ν(C≡C) and the ν(C=C) bands of ***E*-6** at 1972 and 1544 cm^{-1}. (b, c) stepwise re-oxidation of these mixtures at (b) positive potentials of the $\mathbf{7}/\mathbf{7}^+$ and $\mathbf{\textit{E}\text{-}6}/[\mathbf{\textit{E}\text{-}6}]^+$ waves and (c) at positive potentials of the $[7]^+/[7]^{2+}$ and $[\mathbf{\textit{E}\text{-}6}]^+/[\mathbf{\textit{E}\text{-}6}]^{2+}$ waves.

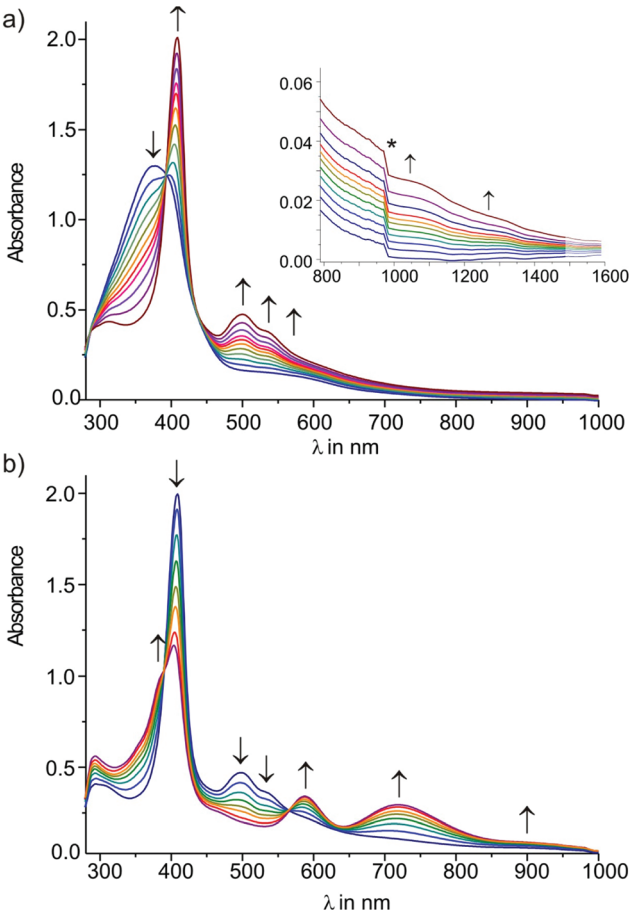

Fig. 10 UV/Vis spectroscopic changes during (a) the first and (b) the second reduction of complex $\mathbf{7[PF_6]_2}$ in THF/NBu_4PF_6 at r.t.

with individual peaks at 498, 533, 588, and 696 nm. In the NIR a much weaker and likewise structured absorption is seen in the 900 to 1500 nm range (see the inset of Fig. 10a). This band is also seen in IR-spectroelectrochemistry as a rising baseline near the high-energy limit of the detector. None of these bands readily qualifies for an IVCT transition of a mixed-valent system. On the other hand structured absorptions of like appearance are routinely seen when redox processes of complexes with carbon-rich ligands produce ligand centered radicals. Alkynyl or vinyl complexes are typical examples.[2o,47a,54] Further reduction to **7** caused an intensity decrease and a splitting of the high-energy band into separate peaks at 358, 390, and 404 nm, as well as the growth of red-shifted bands at 590, 718, and *ca.* 910 nm. Both these steps were largely reversible with *ca.* 90 or 85% optical yields of recovered $[\mathbf{7}]^{2+}$ upon back-electrolysis. Further reduction of **7** produced a solution with the spectroscopic features of complex ***E*-6**, *i.e.* a strong band near 380 nm and an even stronger absorption peaking at 302 nm. Taken together, the emerging picture from our spectro-electrochemical studies is that of ligand dominated reductions of $[\mathbf{7}]^{2+}$ with extensive delocalization of charge and spin over the entire RC≡C–Re–C_4–Re–C≡CR chain and no evidence for a mixed-valent behavior of $[\mathbf{7}]^{+}$. This latter finding is in contrast to other C_4-bridged complexes with more metal centered redox orbitals and also to $[\boldsymbol{E}\text{-}\mathbf{6}]^{+}$.

Conclusions

Starting from the mononuclear rhenium vinylidene complex *trans*-[Re(C≡CSiMe$_3$)(C=CH$_2$)(PMe$_3$)$_4$] (**3**) a series of oxidatively coupled dinuclear complexes *trans*-[(Me$_3$SiC≡C)(PMe$_3$)$_4$ReC$_4$H$_n$Re(PMe$_3$)$_4$(C≡CSiMe$_3$)]$^{m+}$ (n = 2, 0; m = 0, 1, 2) were prepared. For n = 2 and for m = 0 the respective singlet and triplet states ***E*-6(S)** and **7(S)** as well as ***E*-6(S)** and **7(S)** were evaluated. For any of these species it was possible to change the redox state indicated by the charges m = 1,2 of the molecules, which brought about changes in the preferred canonical forms of the bridges. This indicates strong bridge contributions to the respective frontier MOs, *i.e.* a non-innocent character of the C_4H_x-bridges. Oxidation of ***E*-6(S)** to ***E*-6$[\mathbf{PF_6}]_2$** went along with the transformation from a butadienediylidene ([Re]=C=CH–CH=C=[Re]) into an ethylenylidene(ditriyl) ([Re]≡C–CH=CH–C≡[Re]) valence structure. The MV complex of this series of compounds has a large K_c of 7.1 × 10^7, high electronic coupling energy H_{ab} and a high delocalization parameter Γ and can be safely described as a class III MV compound with an intrinsically delocalized {[M]–π-bridge–[M]}$^{+}$ entity. The diradical and the cumulenic closed-shell isomers ([Re](·)=C–C≡C–C=(·)[Re]) **7(F)** ([Re]=C=C=C=C=[Re]) **7(S)** are calculated to be close to isoenergetic. Due to the instability of these species, they could not be fully characterized so no firm conclusion on the prevalent ground state structure can be drawn. By hydrogen abstraction **7** transforms into ***E*-6(S)**. Cyclic voltammetry (CV) studies and IR- and UV-Vis-NIR-spectro-electrochemistry studies for the reduction of **7** $[\mathbf{PF_6}]_2$ revealed a large K_c of 4.7 × 10^8 and hence a high thermodynamic stability of the radical monocation **7**$[\mathbf{PF_6}]$. Structured bands in the visible and NIR of **7**$[\mathbf{PF_6}]$ are indicative of a strongly ligand-centered rather than a purely rhenium centered radical, thus defying its classification as a classical mixed-valent species. Further studies are ongoing in our group for functionalization of the terminal group of ***E*-6** and **7** with the appropriate end groups sticking to gold electrodes suitable for single molecule conductance measurements.

Acknowledgements

Funding from the University of Zurich is gratefully acknowledged. We thank Dr Thomas Fox for his help with the NMR studies.

Notes and references

1 A. Burgun, F. Gendron, C. J. Sumby, T. Roisnel, O. Cador, K. Costuas, J. F. Halet, M. I. Bruce and C. Lapinte, *Organometallics*, 2014, **33**, 2613–2627.

2 (*a*) M. I. Bruce, M. L. Cole, K. Costuas, B. G. Ellis, K. A. Kramarczuk, C. Lapinte, B. K. Nicholson, G. J. Perkins, B. W. Skelton, A. H. White and N. N. Zaitseva, *Z. Anorg. Allg. Chem.*, 2013, **639**, 2216–2223; (*b*) F. Schwarz, G. Kastlunger, F. Lissel, H. Riel, K. Venkatesan, H. Berke, R. Stadler and E. Lortscher, *Nano Lett.*, 2014, **14**, 5932–5940; (*c*) F. Lissel, F. Schwarz, O. Blacque, H. Riel, E. Lortscher, K. Venkatesan and H. Berke, *J. Am. Chem. Soc.*, 2014, **136**, 14560–14569; (*d*) T. Tanaka and A. Osuka, *Chem. Soc. Rev.*, 2015, **44**, 943–969; (*e*) E. Leary, A. La Rosa, M. T. Gonzalez, G. Rubio-Bollinger, N. Agrait and N. Martin, *Chem. Soc. Rev.*, 2015, **44**, 920–942; (*f*) D. M. Guldi, H. Nishihara and L. Venkataraman, *Chem. Soc. Rev.*, 2015, **44**, 842–844; (*g*) S. Rigaut, *Dalton Trans.*, 2013, **42**, 15859–15863; (*h*) J. R. Heath, *Annu. Rev. Mater. Res.*, 2009, **39**, 1–23; (*i*) R. L. Carroll and C. B. Gorman, *Angew. Chem., Int. Ed.*, 2002, **41**, 4379–4400; (*j*) N. J. Tao, *Nat. Nanotechnol.*, 2006, **1**, 173–181; (*k*) F. Chen, J. Hihath, Z. F. Huang, X. L. Li and N. J. Tao, *Annu. Rev. Phys. Chem.*, 2007, **58**, 535–564; (*l*) V. V. Zhirnov and R. K. Cavin, *Nat. Mater.*, 2006, **5**, 11–12; (*m*) T. Kurita, Y. Nishimori, F. Toshimitsu, S. Muratsugu, S. Kume and H. Nishihara, *J. Am. Chem. Soc.*, 2010, **132**, 4524–4525; (*n*) N. Tuccitto, V. Ferri, M. Cavazzini, S. Quici, G. Zhavnerko, A. Licciardello and M. A. Rampi, *Nat. Mater.*, 2009, **8**, 41–46; (*o*) N. Szesni, M. Drexler, J. Maurer, R. F. Winter, F. de Montigny, C. Lapinte, S. Steffens, J. Heck, B. Weibert and H. Fischer, *Organometallics*, 2006, **25**, 5774–5787; (*p*) W. Kaim and G. K. Lahiri, *Angew. Chem., Int. Ed.*, 2007, **46**, 1778–1796; (*q*) K. Kowalski, M. Linseis, R. F. Winter, M. Zabel, S. Záliš, H. Kelm, H. J. Krüger, B. Sarkar and W. Kaim, *Organometallics*, 2009, **28**, 4196–4209; (*r*) F. Paul

and C. Lapinte, *Coord. Chem. Rev.*, 1998, **178**, 431–509; (*s*) P. Belser, S. Bernhard, C. Blum, A. Beyeler, L. De Cola and V. Balzani, *Coord. Chem. Rev.*, 1999, **192**, 155–169; (*t*) V. Balzani, A. Juris, M. Venturi, S. Campagna and S. Serroni, *Chem. Rev.*, 1996, **96**, 759–833; (*u*) P. F. H. Schwab, M. D. Levin and J. Michl, *Chem. Rev.*, 1999, **99**, 1863–1933.

3 (*a*) H. J. Jiao, K. Costuas, J. A. Gladysz, J. F. Halet, M. Guillemot, L. Toupet, F. Paul and C. Lapinte, *J. Am. Chem. Soc.*, 2003, **125**, 9511–9522; (*b*) R. Dembinski, T. Bartik, B. Bartik, M. Jaeger and J. A. Gladysz, *J. Am. Chem. Soc.*, 2000, **122**, 810–822.

4 H. Song, Y. Kim, Y. H. Jang, H. Jeong, M. A. Reed and T. Lee, *Nature*, 2009, **462**, 1039–1043.

5 M. B. Robin and P. Day, *Prog. Inorg. Chem.*, 1967, **10**, 247.

6 M. Parthey and M. Kaupp, *Chem. Soc. Rev.*, 2014, **43**, 5067–5088.

7 (*a*) P. Aguirre-Etcheverry and D. O'Hare, *Chem. Rev.*, 2010, **110**, 4839–4864; (*b*) A. Ceccon, S. Santi, L. Orian and A. Bisello, *Coord. Chem. Rev.*, 2004, **248**, 683–724; (*c*) H. Adams, P. J. Costa, M. Newell, S. J. Vickers, M. D. Ward, V. Felix and J. A. Thomas, *Inorg. Chem.*, 2008, **47**, 11633–11643.

8 (*a*) K. Venkatesan, T. Fox, H. W. Schmalle and H. Berke, *Organometallics*, 2005, **24**, 2834–2847; (*b*) K. Venkatesan, F. J. Fernandez, O. Blacque, T. Fox, M. Alfonso, H. W. Schmalle and H. Berke, *Chem. Commun.*, 2003, 2006–2008; (*c*) S. Kheradmandan, K. Heinze, H. W. Schmalle and H. Berke, *Angew. Chem., Int. Ed.*, 1999, **38**, 2270–2273.

9 N. LeNarvor, L. Toupet and C. Lapinte, *J. Am. Chem. Soc.*, 1995, **117**, 7129–7138.

10 (*a*) M. Brady, W. Q. Weng, Y. L. Zhou, J. W. Seyler, A. J. Amoroso, A. M. Arif, M. Böhme, G. Frenking and J. A. Gladysz, *J. Am. Chem. Soc.*, 1997, **119**, 775–788; (*b*) Y. L. Zhou, J. W. Seyler, W. Q. Weng, A. M. Arif and J. A. Gladysz, *J. Am. Chem. Soc.*, 1993, **115**, 8509–8510; (*c*) V. W. W. Yam, V. C. Y. Lau and K. K. Cheung, *Organometallics*, 1996, **15**, 1740–1744.

11 (*a*) M. I. Bruce, P. J. Low, K. Costuas, J. F. Halet, S. P. Best and G. A. Heath, *J. Am. Chem. Soc.*, 2000, **122**, 1949–1962; (*b*) F. Paul, W. E. Meyer, L. Toupet, H. J. Jiao, J. A. Gladysz and C. Lapinte, *J. Am. Chem. Soc.*, 2000, **122**, 9405–9414.

12 K. Onitsuka, N. Ose, F. Ozawa and S. Takahashi, *J. Organomet. Chem.*, 1999, **578**, 169–177.

13 (*a*) B. E. Woodworth, P. S. White and J. L. Templeton, *J. Am. Chem. Soc.*, 1997, **119**, 828–829; (*b*) R. L. Roberts, H. Puschmann, J. A. K. Howard, J. H. Yamamoto, A. J. Carty and P. J. Low, *Dalton Trans.*, 2003, 1099–1105; (*c*) S. N. Semenov, O. Blacque, T. Fox, K. Venkatesan and H. Berke, *J. Am. Chem. Soc.*, 2010, **132**, 3115–3127.

14 M. Gulcur, P. Moreno-Garcia, X. T. Zhao, M. Baghernejad, A. S. Batsanov, W. J. Hong, M. R. Bryce and T. Wandlowski, *Chem. – Eur. J.*, 2014, **20**, 4653–4660.

15 X. T. Zhao, C. C. Huang, M. Gulcur, A. S. Batsanov, M. Baghernejad, W. J. Hong, M. R. Bryce and T. Wandlowski, *Chem. Mater.*, 2013, **25**, 4340–4347.

16 (*a*) A. Kuzume, U. Zhumaev, J. F. Li, Y. C. Fu, M. Fueg, M. Estevez, Z. Borjas, T. Wandlowski and A. Esteve-Nunez, *Phys. Chem. Chem. Phys.*, 2014, **16**, 22229–22236; (*b*) W. J. Hong, H. Li, S. X. Liu, Y. C. Fu, J. F. Li, V. Kaliginedi, S. Decurtins and T. Wandlowski, *J. Am. Chem. Soc.*, 2012, **134**, 19425–19431.

17 K. Costuas and S. Rigaut, *Dalton Trans.*, 2011, **40**, 5643–5658.

18 (*a*) L. N. Novikova, M. G. Peterleitner, K. A. Sevumyan, O. V. Semeikin, D. A. Valyaev and N. A. Ustynyuk, *Appl. Organomet. Chem.*, 2002, **16**, 530–536; (*b*) N. A. Ustynyuk, O. V. Gusev, L. N. Novikova, M. G. Peterleitner, L. I. Denisovich, T. A. Peganova, O. V. Semeikin and D. A. Valyaev, *J. Solid State Electrochem.*, 2007, **11**, 1621–1634.

19 (*a*) R. P. Orenha, R. Vessecchi and S. E. Galembeck, *Struct. Chem.*, 2015, **26**, 365–373; (*b*) A. A. Zavitsas, N. Matsunaga and D. W. Rogers, *J. Phys. Chem. A*, 2008, **112**, 5734–5741.

20 T. Flitcroft, H. A. Skinner and M. C. Whiting, *Trans. Faraday Soc.*, 1957, **53**, 784–790.

21 (*a*) W. Kaim, *Inorg. Chem.*, 2011, **50**, 9752–9765; (*b*) W. Kaim, *Eur. J. Inorg. Chem.*, 2012, 343–348; (*c*) S. Záliš, R. F. Winter and W. Kaim, *Coord. Chem. Rev.*, 2010, **254**, 1383–1396; (*d*) M. D. Ward and J. A. McCleverty, *J. Chem. Soc., Dalton Trans.*, 2002, 275–288; (*e*) P. Comba, A. Hauser, M. Kerscher and H. Pritzkow, *Angew. Chem., Int. Ed.*, 2003, **42**, 4536–4540.

22 (*a*) G. Parkin, *Acc. Chem. Res.*, 1992, **25**, 455–460; (*b*) Y. Jean, A. Lledos, J. K. Burdett and R. Hoffmann, *J. Am. Chem. Soc.*, 1988, **110**, 4506–4516; (*c*) J. A. Labinger, *C. R. Chim.*, 2002, **5**, 235–244.

23 (*a*) F. J. Fernandez, M. Alfonso, H. W. Schmalle and H. Berke, *Organometallics*, 2001, **20**, 3122–3131; (*b*) F. J. Fernandez, K. Venkatesan, O. Blacque, M. Alfonso, H. W. Schmalle and H. Berke, *Chem. – Eur. J.*, 2003, **9**, 6192–6206; (*c*) S. Kheradmandan, K. Venkatesan, O. Blacque, H. W. Schmalle and H. Berke, *Chem. – Eur. J.*, 2004, **10**, 4872–4885; (*d*) K. Venkatesan, O. Blacque and H. Berke, *Dalton Trans.*, 2007, 1091–1100; (*e*) K. Venkatesan, O. Blacque, T. Fox, M. Alfonso, H. W. Schmalle and H. Berke, *Organometallics*, 2004, **23**, 1183–1186; (*f*) K. Venkatesan, O. Blacque, T. Fox, M. Alfonso, H. W. Schmalle, S. Kheradmandan and H. Berke, *Organometallics*, 2005, **24**, 920–932.

24 (*a*) K. Venkatesan, O. Blacque and H. Berke, *Organometallics*, 2006, **25**, 5190–5200; (*b*) D. Unseld, V. V. Krivykh, K. Heinze, F. Wild, G. Artus, H. Schmalle and H. Berke, *Organometallics*, 1999, **18**, 1525–1541.

25 A. Antiñolo, A. Otero, M. Fajardo, C. García-Yebra, C. López-Mardomingo, A. Martín and P. Gómez-Sal, *Organometallics*, 1997, **16**, 2601–2611.

26 R. L. Beddoes, C. Bitcon, R. W. Grime, A. Ricalton and M. W. Whiteley, *J. Chem. Soc., Dalton Trans.*, 1995, 2873–2883.

27 L. N. Novikova, M. G. Peterleitner, K. A. Sevumyan, O. V. Semeikin, D. A. Valyaev, N. A. Ustynyuk,

V. N. Khrustalev, L. N. Kuleshova and M. Y. Antipin, *J. Organomet. Chem.*, 2001, **631**, 47–53.
28 D. A. Valyaev, O. V. Semelkin, M. G. Peterleitner, Y. A. Borisov, V. N. Khrustalev, A. M. Mazhuga, E. V. Kremer and N. A. Ustynyuk, *J. Organomet. Chem.*, 2004, **689**, 3837–3846.
29 R. S. Iyer and J. P. Selegue, *J. Am. Chem. Soc.*, 1987, **109**, 910–911.
30 M. I. Bruce, B. G. Ellis, P. J. Low, B. W. Skelton and A. H. White, *Organometallics*, 2003, **22**, 3184–3198.
31 (*a*) M. I. Bruce, *Chem. Rev.*, 1991, **91**, 197–257; (*b*) D. A. Valyaev, O. V. Semeikin and N. A. Ustynyuk, *Coord. Chem. Rev.*, 2004, **248**, 1679–1692; (*c*) C. Bruneau and P. Dixneuf, *Metal Vinylidenes and Allenylidenes in Catalysis: From Reactivity to Application in Synthesis*, Wiley-VCH Verlag GmbH & Co. KgaA, Weinheim, 2008; (*d*) H. Werner, *Coord. Chem. Rev.*, 2004, **248**, 1693–1702.
32 (*a*) M. Newcomb and M. T. Burchill, *J. Am. Chem. Soc.*, 1984, **106**, 8276–8282; (*b*) M. Newcomb and M. T. Burchill, *J. Am. Chem. Soc.*, 1984, **106**, 2450–2451; (*c*) M. Jasinski, G. Mloston, A. Gebert and H. Heimgartner, *Phosphorus, Sulfur Silicon Relat. Elem.*, 2015, **190**, 1281–1284.
33 T. A. Albright, J. Burdettt and M. Whangbo, *Orbital Interactions in Chemistry*, John Wiley & Sons, Inc., Hoboken, New Jersey, USA, 2013.
34 A. J. L. Pombeiro, A. Hills, D. L. Hughes and R. L. Richards, *J. Organomet. Chem.*, 1988, **352**, C5–C7.
35 D. R. Lide and H. P. Frederikse, *CRC Handbook of Chemistry and Physics*, CRC press, Boca Raton, 1995.
36 (*a*) A. D. Becke, *Phys. Rev. A*, 1988, **38**, 3098–3100; (*b*) C. T. Lee, W. T. Yang and R. G. Parr, *Phys. Rev. B: Condens. Matter*, 1988, **37**, 785–789; (*c*) A. D. Becke, *J. Chem. Phys.*, 1993, **98**, 1372–1377.
37 (*a*) M. Renz and M. Kaupp, *J. Phys. Chem. A*, 2012, **116**, 10629–10637; (*b*) M. Renz, K. Theilacker, C. Lambert and M. Kaupp, *J. Am. Chem. Soc.*, 2009, **131**, 16292–16302; (*c*) M. Renz, M. Kess, M. Diedenhofen, A. Klamt and M. Kaupp, *J. Chem. Theory Comput.*, 2012, **8**, 4189–4203.
38 (*a*) V. Coropceanu, C. Lambert, G. Nöll and J. L. Brédas, *Chem. Phys. Lett.*, 2003, **373**, 153–160; (*b*) V. Coropceanu, M. Malagoli, J. M. Andre and J. L. Brédas, *J. Am. Chem. Soc.*, 2002, **124**, 10519–10530.
39 (*a*) J. P. Perdew and Y. Wang, *Phys. Rev. B: Condens. Matter*, 1992, **45**, 13244–13249; (*b*) J. P. Perdew, K. Burke and M. Ernzerhof, *Phys. Rev. Lett.*, 1996, **77**, 3865–3868; (*c*) J. P. Perdew, M. Ernzerhof and K. Burke, *J. Chem. Phys.*, 1996, **105**, 9982–9985.
40 A. D. Becke, *J. Chem. Phys.*, 1993, **98**, 5648–5652.
41 J. P. Perdew, *Phys. Rev. B: Condens. Matter*, 1986, **33**, 8822–8824.
42 P. Gütlich, H. A. Goodwin and D. N. Hendrickson, *Angew. Chem., Int. Ed.*, 1994, **33**, 425–427.
43 E. Ruiz, J. Cirera and S. Alvarez, *Coord. Chem. Rev.*, 2005, **249**, 2649–2660.
44 S. Le Stang, F. Paul and C. Lapinte, *Organometallics*, 2000, **19**, 1035–1043.
45 (*a*) D. M. D'Alessandro and F. R. Keene, *Chem. Soc. Rev.*, 2006, **35**, 424–440; (*b*) K. D. Demadis, C. M. Hartshorn and T. J. Meyer, *Chem. Rev.*, 2001, **101**, 2655–2685.
46 J. R. Reimers and N. S. Hush, *Inorg. Chem.*, 1990, **29**, 4510–4513.
47 (*a*) W. Y. Man, J. L. Xia, N. J. Brown, J. D. Farmer, D. S. Yufit, J. A. K. Howard, S. H. Liu and P. J. Low, *Organometallics*, 2011, **30**, 1852–1858; (*b*) F. Lissel, T. Fox, O. Blacque, W. Polit, R. F. Winter, K. Venkatesan and H. Berke, *J. Am. Chem. Soc.*, 2013, **135**, 4051–4060.
48 (*a*) N. S. Hush, *Coord. Chem. Rev.*, 1985, **64**, 135–157; (*b*) N. S. Hush, *Prog. Inorg. Chem.*, 1967, 391.
49 B. S. Brunschwig, C. Creutz and N. Sutin, *Chem. Soc. Rev.*, 2002, **31**, 168–184.
50 J. A. Weil and J. R. Bolton, *Electron Paramagnetic Resonance: Elementary Theory and Practical Applications*, Wiley, New York, 1994.
51 (*a*) W. Q. Weng, T. Bartik, M. Brady, B. Bartik, J. A. Ramsden, A. M. Arif and J. A. Gladysz, *J. Am. Chem. Soc.*, 1995, **117**, 11922–11931; (*b*) J. W. Seyler, W. Q. Weng, Y. L. Zhou and J. A. Gladysz, *Organometallics*, 1993, **12**, 3802–3804.
52 C. Herrmann, J. Neugebauer, J. A. Gladysz and M. Reiher, *Inorg. Chem.*, 2005, **44**, 6174–6182.
53 (*a*) M. I. Bruce, K. Costuas, T. Davin, B. G. Ellis, J. F. Halet, C. Lapinte, P. J. Low, M. E. Smith, B. W. Skelton, L. Toupet and A. H. White, *Organometallics*, 2005, **24**, 3864–3881; (*b*) M. I. Bruce, K. Costuas, T. Davin, J. F. Halet, K. A. Kramarczuk, P. J. Low, B. K. Nicholson, G. J. Perkins, R. L. Roberts, B. W. Skelton, M. E. Smith and A. H. White, *Dalton Trans.*, 2007, 5387–5399.
54 (*a*) M. A. Fox, R. L. Roberts, W. M. Khairul, F. Hartl and P. J. Low, *J. Organomet. Chem.*, 2007, **692**, 3277–3290; (*b*) M. A. Fox, J. D. Farmer, R. L. Roberts, M. G. Humphrey and P. J. Low, *Organometallics*, 2009, **28**, 5266–5269; (*c*) N. Gauthier, N. Tchouar, F. Justaud, G. Argouarch, M. P. Cifuentes, L. Toupet, D. Touchard, J. F. Halet, S. Rigaut, M. G. Humphrey, K. Costuas and F. Paul, *Organometallics*, 2009, **28**, 2253–2266; (*d*) J. Maurer, R. F. Winter, B. Sarkar, J. Fiedler and S. Zalis, *Chem. Commun.*, 2004, 1900–1901; (*e*) J. Maurer, M. Linseis, B. Sarkar, B. Schwederski, M. Niemeyer, W. Kaim, S. Zalis, C. Anson, M. Zabel and R. F. Winter, *J. Am. Chem. Soc.*, 2008, **130**, 259–268; (*f*) J. Maurer, B. Sarkar, B. Schwederski, W. Kaim, R. F. Winter and S. Záliš, *Organometallics*, 2006, **25**, 3701–3712; (*g*) F. Pevny, E. Di Piazza, L. Norel, M. Drescher, R. F. Winter and S. Rigaut, *Organometallics*, 2010, **29**, 5912–5918.